Asymptotic rate of quantum ergodicity in chaotic Euclidean billiards

Alex H. Barnett

Courant Institute, New York University, 251 Mercer St, New York, NY 10012

barnett@cims.nyu.edu

July 3, 2004

Abstract

The Quantum Unique Ergodicity (QUE) conjecture of Rudnick-Sarnak is that every quantum (Laplace) eigenfunction ϕ_n of an ergodic, uniformly-hyperbolic classical geodesic flow becomes equidistributed in the semiclassical limit (eigenvalue $E_n \to \infty$). We report numerical results on the rate of quantum ergodicity, for a uniformly-hyperbolic Euclidean billiard with Dirichlet boundary condition (the 'drum problem') at unprecedented high E and statistical accuracy. We calculate matrix elements $\langle \phi_n, \hat{A}\phi_m \rangle$ of a piecewise-constant test observable A, and collect 30000 diagonal matrix elements up to level $n \approx 7\times 10^5$. Our results support the validity of QUE, that is, there are no 'strong scars'. We find asymptotic power-law decay $aE^{-\gamma}$ of the diagonal variance with $\gamma \approx 0.48 \pm 0.01$. However convergence to the semiclassical estimate of Feingold-Peres (FP), where $\gamma = 1/2$, appears slow. We also compare off-diagonal variance with the FP sum rule at the highest accuracy (0.7%) known in any chaotic system.

1 Introduction

The nature of the quantum mechanics of Hamiltonian systems whose classical counterparts are chaotic has been of long-standing interest, dating back to Einstein in 1917 (see [51] for a historical account). The field now called 'quantum chaos' is the study of such quantized systems in the short wavelength

(semiclassical, $\hbar \to 0$ or high energy) regime, and has become a fruitful area of enquiry for both physicists and mathematicians in recent decades [29, 31]. A central issue is the behaviour of the eigenfunctions, which in contrast to the regular eigenfunctions resulting from integrable classical motion, are irregular.

In 1977 Berry [12] put forward the conjecture that chaotic eigenfunctions should look locally like a random superposition of plane waves at all angles and fixed (locally appropriate) energy, and that their Wigner functions tend to the classical ergodic invariant measure (Liouville measure) on the constant-energy hypersurface in phase space. This can be thought of as 'quantum ergodic' behaviour of the eigenfunctions. (See Figs. 2 and 3 for a visual comparison of a random wave with an actual eigenfunction, also see [31]). The resulting Gaussian distribution of coordinate space wavefunction values would also be predicted by Random Matrix Theory (RMT), assuming that it is valid for such chaotic systems [16]. Numerical quantum calculations in a strongly-chaotic system were absent until the pioneering work of McDonald and Kaufman [41] on the two-dimensional (2D) stadium billiard, which verified the eigenvalue repulsion predicted by RMT, and showed angular isotropy for some irregular eigenfunctions. The classical billiard problem in 2D is the free motion of a point particle bouncing elastically off the boundary Γ of a bounded domain $\Omega \subset \mathbb{R}^2$. The phase space coordinate is $(\mathbf{r}, \theta) \in \Omega \times S^1$, with position coordinate $\mathbf{r} := (x, y)$ and momentum direction θ. We assume constant (unit) speed. The quantum version is the Laplace eigenproblem [34], also known as the membrane or drum problem,

$$-\Delta \phi_n = E_n \phi_n, \tag{1}$$

$$\phi_n(\Gamma) = 0, \tag{2}$$

with homogeneous boundary conditions here chosen to be Dirichlet. Eigenfunctions $\phi_n(\mathbf{r})$ are normalized

$$\langle \phi_n, \phi_m \rangle = \delta_{nm}, \tag{3}$$

and the corresponding eigenvalues ordered $E_1 \leq E_2 \leq \cdots$. Our units are such that $E = k^2$ where the wavenumber is $k = 2\pi/\lambda$, the wavelength being λ. This problem has a rich 150-year history of application to acoustics, electromagnetism, mechanical vibration, quantum mechanics, and optics, to name a few areas. In keeping with quantum-mechanical terminology we will say that level n has energy E_n.

Analytical results on quantum ergodicity in hyperbolic manifolds without boundary (where the Laplacian is replaced by its curved-space generalization) originated with Schnirelman [48] and was carried through by Zelditch [56] and Colin de Verdière [21]. These results make use of microlocal analysis (for reviews see [5, 46, 38]), and study a pseudodifferential operator (for a physicist, a quantum observable) $\hat{A}$ acting on quantum wavefunctions, and its corresponding classical Weyl symbol $A(\mathbf{r}, \theta)$ (a function of phase space). The case of billiards with a boundary was proven by Zelditch and Zworski [58], and can be stated as

Theorem 1 (Quantum Ergodicity Theorem (QET) [58]) *Let $\Omega \in \mathbb{R}^2$ be a 2D compact domain with piecewise smooth boundary whose classical flow is ergodic, and whose orthonormal Dirichlet Laplace eigenfunctions are ϕ_n. Then there exists a subsequence $n_j \subset \mathbb{N}$ of density one for which*

$$\langle \phi_{n_j}, \hat{A}\phi_{n_j} \rangle - \overline{A} \to 0 \qquad as \quad j \to \infty, \tag{4}$$

for all well-behaved [58] observables $A(\mathbf{r}, \theta)$.

A subsequence is said to have density one if $\#\{j : n_j \leq N\}/N \to 1$ as $N \to \infty$. We call $\langle \phi_n, \hat{A}\phi_n \rangle$ a diagonal matrix element, or quantum expectation of A in the pure state ϕ_n. The classical expectation is the phase space average $\overline{A}$, which in the case of momentum-independent $A = A(\mathbf{r})$ is

$$\overline{A} \;=\; \frac{1}{\mathrm{vol}(\Omega)} \int_\Omega A(\mathbf{r})\, d\mathbf{r}\,, \tag{5}$$

where $d\mathbf{r} = dxdy$ is the area element. $\overline{A}$ is independent of energy because for billiards the Hamiltonian obeys a scaling law (dynamics is the same at any energy). Note that the Weyl law for the level density the equivalence of $n \to \infty$ and $E_n \to \infty$. Asymptotic equality of quantum and classical expectations for all observables A is known to physicists as the Correspondence Principle. (In the semiclassical limit only local energy averages, rather than individual pure states, are physically accessible, so an exceptional sequence of vanishing density has no effect on measurable quantities). QET implies [21] that the mass measure (the usual quantum interpretation being probability density, or 'intensity') $d\mu_{\phi_n} := |\phi_n|^2\, d\mathbf{r}$ tends (in the weak sense) to the uniform measure $d\mathbf{r}/\mathrm{vol}(\Omega)$, in other words that mass becomes equidistributed in the semiclassical limit, for almost all n. $A(\mathbf{r})$ can be viewed as a 'test function' which measures equidistribution.

The discovery by Heller [30, 31] that a large fraction of stadium eigenfunctions showed strong visible enhancement near classical unstable periodic orbits (UPOs) was therefore a surprise. Heller dubbed these localized features 'scars' and put forward a semiclassical explanation based on enhanced short-time return probability for wavepackets launched along the least unstable UPOs. The theory has been expanded [14, 13, 1, 39]. Although the meaning of 'scar' has varied historically, it is now taken to mean *any* deviation from the RMT prediction of eigenfunction intensity near a UPO [39]. As reviewed by Kaplan and Heller [40], scar strength depends on what test function you use to measure it: in most quantum chaos literature this test function is *not* held fixed as the limit $E \to \infty$ is taken, rather it is chosen to collapse onto the orbit with a width $\sim E^{-1/4}$. With this measure, scar strength need not die out in the semiclassical limit (indeed it is believed not to [39]) however for any fixed coordinate-space test function $A(\mathbf{r})$ deviations in $\langle \phi_n, \hat{A}\phi_n \rangle$ will do so. 'Strong scarring' we will define to mean an $O(1)$ deviation of total probability mass in the neighborhood of a UPO, equivalently an $O(1)$ deviation in $\langle \phi_n, \hat{A}\phi_n \rangle$. (Asymptotically this coincides with the usage of [44]).

Heller's numerical calculations were done at the seemingly large quantum number $n \approx 2 \times 10^3$ (for the desymmetrized quarter-stadium or 8×10^3 for the full stadium). It is now believed to be likely [1, 39, 35] that in 2D billiards strong scarring dies out in the semiclassical limit, but the issue remains open. There still exist controversies about the width of scars [35], and in related quantum models the mechanism of scarring is an active research area [47]. Bear in mind that QET allows for a sequence of strongly-scarred states to persist asymptotically as long as their density tends to zero. Scarring is not to be confused with the set of eigenfunctions which concentrates about a family of neutrally-stable periodic orbits. Such 'bouncing ball' modes (similar in form to EBK-quantized integrable modes [29]) are present in the stadium, and are believed to persist asymptotically as a sequence with density vanishing algebraically [52, 4], although this is not known rigorously [24]. To remove this complication we confine our discussion to Anosov systems (uniformly hyperbolic, or 'hard chaos' in the sense of [29]), that is, all UPOs are isolated and all Lyapunov exponents bounded away from zero. This excludes for example the stadium.

A much stronger conjecture than QET has been made by Rudnick and Sarnak in the context of negatively-curved (Anosov) manifolds, namely

Conjecture 1 (Quantum Unique Ergodicity (QUE) [44]) *As the semiclassical limit is reached,* every *eigenfunction* ϕ_n *becomes equidistributed. That is,*

$$\langle \phi_n, \hat{A}\phi_n \rangle - \overline{A} \to 0 \qquad as \quad n \to \infty, \tag{6}$$

for all well-behaved observables $A(\mathbf{r}, \theta)$.

Any limit of the measure $d\mu_{\phi_n}$ is called a 'quantum limit'. It is known that any quantum limit must be invariant under the classical flow [48, 21, 56]. This leaves open the possibility of arc-length measure along any UPOs, or combinations thereof, as (singular) quantum limits. The adjective 'unique' in QUE refers to only one possible quantum limit occurring: the uniform measure. QUE implies that not a single strong scar persists in the semiclassical limit. In 'arithmetic' manifolds, questions about eigenfunctions are accessible analytically due to the presence of a special set of Hecke operators which commute with the Hamiltonian [44, 45]. For these manifolds it was known that singular quantum limits could not exist [44], and, remarkably, QUE has recently been proved [36]. However, QUE for general manifolds such as Euclidean billiards, where ergodicity results from the presence of a boundary, remains a conjecture. Note that, in contrast, QUE has been proven not to hold for certain-dimensional quantizations of Arnold's cat map, another paradigm quantum chaotic system [26].

Arithmetic manifolds are very special systems: all Lyapunov exponents are equal, and they are highly symmetric; for instance this results in eigenvalue spectrum statistics entirely different from RMT predictions [15]. Therefore it is valid to question what if any results from the arithmetic case carry over to more generic systems. In this work we collect numerical evidence for equidistribution and the validity of QUE in a much more generic system, namely a 2D Euclidean billiard, Anosov, with no symmetry and differing Lyapunov exponents. We will study the variance of diagonal matrix elements $\langle \phi_n, \hat{A}\phi_n \rangle$, and the rate of equidistribution, namely how this variance decays to zero as $E \to \infty$. We compare this rate to the semiclassical estimate first formulated by Feingold and Peres [27] (we will call FP) involving the time-integrated auto-correlation (the 'classical variance') of the function A under the geodesic flow (classical evolution). There are several approaches to FP, which we review in Section 2.2. Studying this rate is important firstly because it determines the practical applicability of the QET. Secondly, recent analytic work in arithmetic systems includes the result that the classical variance *provably* differs from the true rate, even in the asymptotic limit, in

a fashion that depends on the choice of A [46, 37]. It is therefore of great interest whether the FP estimate holds for more generic systems, such as billiards.

We know of only one serious numerical study [5] of equidistribution rate in Euclidean billiards. This was limited to quantum numbers $n < 6000$, a range similar to the original work of Heller [30] where strong scarring appears very common. This fact alone suggests that the study is unlikely to have reached any asymptotic regime; we will present evidence later that supports this suggestion. Billiards allow extremely efficient numerical methods for finding eigenfunctions that enable us to perform a large-scale study of equidistribution rate, for certain observables A, with very high (and quantified) statistical accuracy; we will reach 100 times higher in n than the previous work. Since FP also involves a prediction for variance of *off-diagonal* matrix elements, which we can also efficiently calculate, we will compare the off-diagonal variance to FP, again with very high accuracy.

The rest of this paper is laid out as follows. In Section 2 we present semiclassical rate estimates, first a crude estimate based on the random-wave model, then a derivation of the FP result making use of the QET, finally a review of numerical tests of FP in the literature. Section 3 describes the system we study and overviews the extremely efficient numerical methods used for the quantum calculation. Section 4 contains our numerical results on QUE and ergodicity rate for diagonal elements, followed by results on off-diagonal elements. We discuss competing interpretations of the data, and the effect of the boundary, in Section 5. We summarize our conclusions in Section 6. Two appendices give further details of our numerical calculation methods: Appendix A explains the classical calculations, and Appendix B outlines how quantum eigenfunctions are found efficiently. We also point the reader to the companion paper [10] which contains proof of a theorem which plays a key role in the method for quantum eigenfunctions. The appendix of [10] also contains the proof of an overlap identity used in Section 3.1 of the present work, which is essential for the efficient calculation of matrix elements.

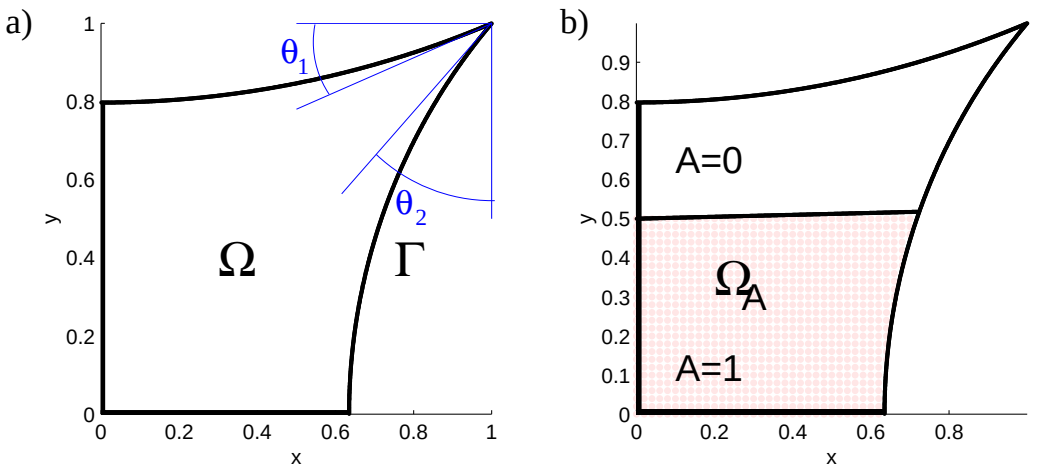

Figure 1: Geometry of billiard and test function used in this study. a) shows quarter generalized Sinai billiard formed from circular arcs which meet at the location $(1, 1)$ at angles $\theta_1 = 0.4$ to the horizontal and $\theta_2 = 0.7$ to the vertical. The arcs intersect the straight sections at right angles. The area is $\mathrm{vol}(\Omega) \approx 0.6140$. b) shows piecewise-constant $A(\mathbf{r})$ which takes the value 1 inside the region Ω_A and zero elsewhere. The 'chop' line is straight and has general orientation.

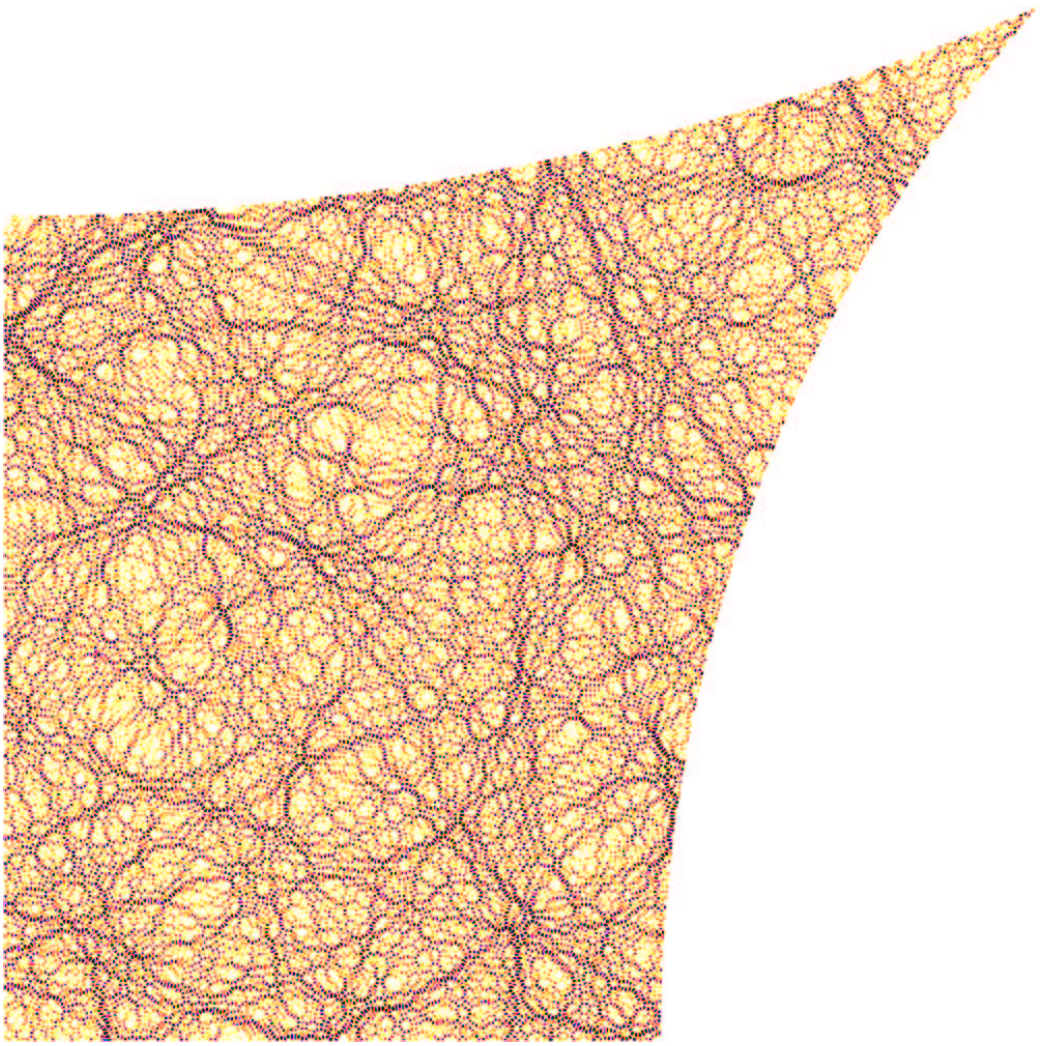

Figure 2: An eigenfunction $\phi_n(\mathbf{r})$ of the billiard under study, with $k_n = 999.90598\cdots$, that is, $E_n \approx 10^6$, and level number $n \approx 5 \times 10^4$ (of the desymmetrized system). The plot shows density $|\phi_n(\mathbf{r})|^2$ on a scale where white is zero, and darker are larger values. There are about 225 wavelengths across the diagonal.

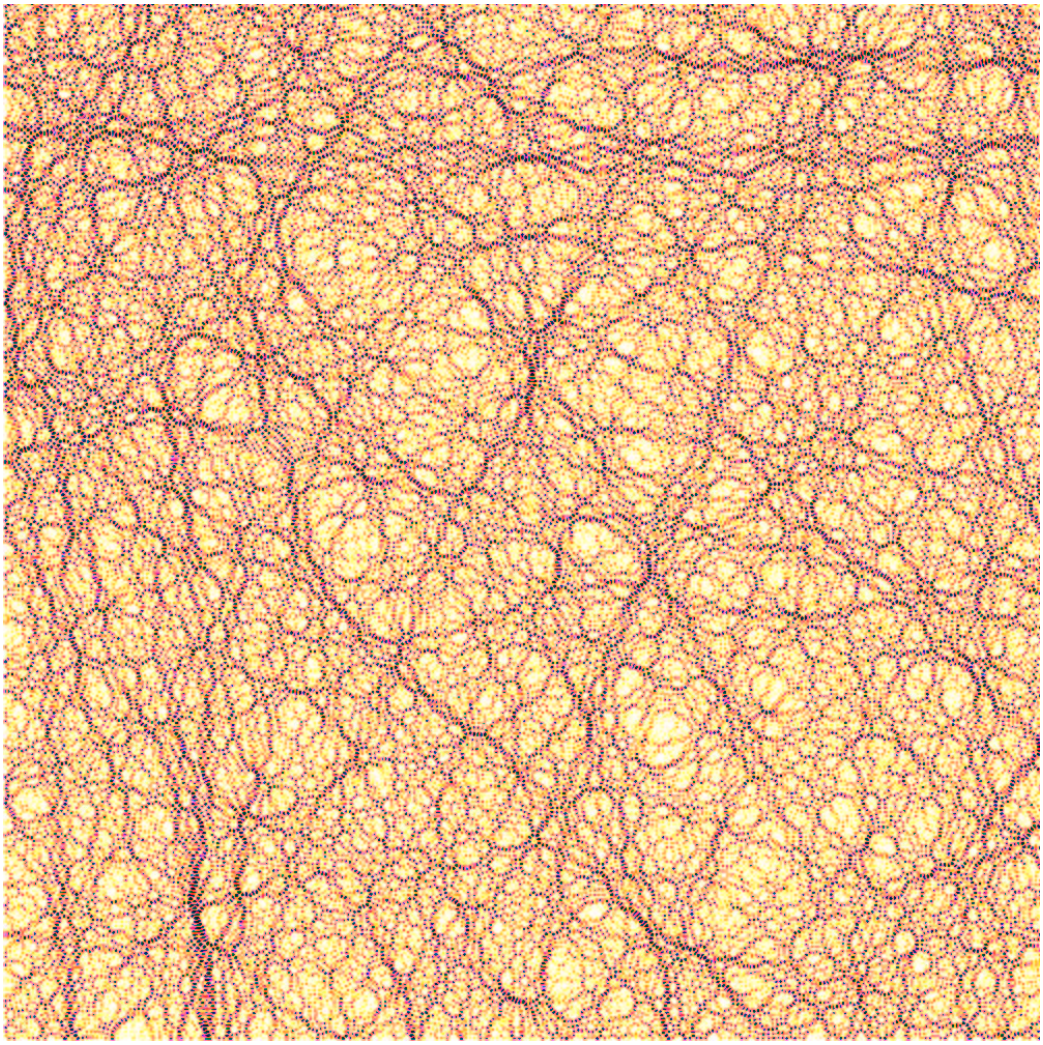

Figure 3: Density plot of a sample from the ensemble of random plane waves with the same wavenumber magnitude $|\mathbf{k}| = k$ and mean intensity as the eigenfunction in Fig. 2, shown over a square region of space. (There are no boundary conditions imposed on the edges of the square). Note that the 'stringy' structures visible to the eye are a feature of the constant wavevector magnitude; they disappear if a range of k is included [31].

2 Ergodicity rate: semiclassical estimates

In this section we summarize some known estimates for the variance of matrix elements. We call the matrix elements $A_{nm} := \langle \phi_n, \hat{A}\phi_m \rangle$, where explicitly,

$$\langle \phi_n, \hat{A}\phi_m \rangle \;:=\; \int_\Omega \phi_n(\mathbf{r})\phi_m(\mathbf{r})A(\mathbf{r})d\mathbf{r}. \tag{7}$$

The variance of diagonal elements we treat as a slowly-varying function of energy, $V_A(E)$. We define it in via a local estimate

$$V_A(E) := \frac{1}{M} \sum_{E_n \approx E}^{N \le n < N+M} \left| \langle \phi_n, \hat{A}\phi_n \rangle - \overline{A} \right|^2, \tag{8}$$

where the interval M contains many levels but remains classically small. That is, $1 \ll M \ll N$, or equivalently, the range of energy is much smaller than E itself. We will define off-diagonal variance below.

2.1 Random wave approach

We first derive and discuss a known result [25] arising from the random wave conjecture. We start with the two-point correlation of a random-wave field [12],

$$\langle \phi(\mathbf{r}_1)\phi(\mathbf{r}_2) \rangle = \frac{1}{\mathrm{vol}(\Omega)} J_0(k|\mathbf{r}_1 - \mathbf{r}_2|), \tag{9}$$

where we use the normalization $\mathrm{vol}(\Omega)\langle \phi^2 \rangle = 1$ appropriate to the billiard volume. This applies to real (time-reversal symmetric) or complex (non time-reversal symmetric) waves; from now we confine ourselves to the real case. Averaging here is defined to be over the ensemble of random plane wave coefficients, with $\mathbf{r}_1$ and $\mathbf{r}_2$ held fixed. Equivalently, the averaging can be taken over a region of space (which should be many wavelengths in size but small compared to the system), with $|\mathbf{r}_1 - \mathbf{r}_2|$ fixed. Because the model is a statistical one, it will be meaningful to speak of the variance of a particular matrix element, namely $\mathrm{var}(A_{nm})$, within the ensemble. A simple calculation using (9) and Wick's theorem for Gaussian random variables gives

$$\langle \phi_n(\mathbf{r}_1)\phi_m(\mathbf{r}_1)\phi_n(\mathbf{r}_2)\phi_m(\mathbf{r}_2) \rangle = \frac{1}{\mathrm{vol}(\Omega)^2} \left[\delta_{nm} + g_{nm} J_0^2(k|\mathbf{r}_1 - \mathbf{r}_2|) \right], \tag{10}$$

where

$$g_{nm} := \begin{cases} g, & n = m, \\ 1, & n \neq m, \end{cases} \quad . \tag{11}$$

The symmetry factor, which we will see shortly gives the ratio of diagonal to off-diagonal variance, is $g = 2$. Its value is associated with time-reversal symmetry (the ratio is a standard result of RMT within the Gaussian Orthogonal Ensemble [16]) combined with the assumption that values of ϕ_n and ϕ_m are statistically independent for $n \neq m$. This latter independence assumption, like the random wave model itself, remains a heuristic one, which also has numerical support. Clearly orthogonality (3) dictates that, when considered as functions over all of Ω, ϕ_n and ϕ_m cannot be independent! However, when restricted to a region much smaller than the billiard volume, independence follows from the RMT conjecture that a set of eigenfunctions behaves like a set of random orthogonal basis vectors drawn from a rotationally-invariant ensemble. (Projections of random orthogonal vectors onto a much smaller-dimensional space become approximately independent). We return to this assumption in step (ii) of the following section.

Now we use (10) to evaluate the variance of both diagonal or off-diagonal matrix elements,

$$\begin{aligned} \mathrm{var}(A_{nm}) &= \langle \left| \int_\Omega \phi_n(\mathbf{r})\phi_m(\mathbf{r})A(\mathbf{r})d\mathbf{r} \right|^2 \rangle \; - \; \langle A_{nm} \rangle^2 \\ &= \frac{g_{nm}}{\mathrm{vol}(\Omega)^2} \iint J_0(k_n|\mathbf{r}_1 - \mathbf{r}_2|) J_0(k_m|\mathbf{r}_1 - \mathbf{r}_2|) d\mathbf{r}_1 d\mathbf{r}_2 \qquad (12) \\ &\approx \frac{g_{nm}}{\pi \mathrm{vol}(\Omega)} E^{-1/2} \iint \frac{A(\mathbf{r}_1)A(\mathbf{r}_2)}{|\mathbf{r}_1 - \mathbf{r}_2|} d\mathbf{r}_1 d\mathbf{r}_2. \qquad (13) \end{aligned}$$

Note that $\langle A_{nm} \rangle = \delta_{nm} \overline{A}$. In the final step two approximations have been made: i) $L|k_n - k_m| \ll 1$ where L is the largest spatial scale of $A(\mathbf{r})$, meaning that the two Bessel functions always remain in phase so can be set equal, and ii) the asymptotic form $J_0(x) \sim (2/\pi x)^{1/2} \cos(x - \pi/4)$ was used, and $\cos^2$ replaced by its average value $\frac{1}{2}$, giving a semiclassical expression valid when $kl \gg 1$, where l is the smallest relevant spatial scale in $A(\mathbf{r})$. Thus we have

$$\mathrm{var}(A_{nn}) = g \, \mathrm{var}(A_{nm}) \tag{14}$$

in a region $n \approx m$ close enough to the diagonal. Returning to the diagonal case we have a power law in energy,

$$V_A(E) \; \approx \; a_{\mathrm{RW}} E^{-1/2}, \tag{15}$$

where the prefactor takes the form of the Coulomb interaction energy of the 'charge density' $A(\mathbf{r})$,

$$a_{\mathrm{RW}} = \frac{g}{\pi \mathrm{vol}(\Omega)} \iint \frac{A(\mathbf{r}_1)A(\mathbf{r}_2)}{|\mathbf{r}_1 - \mathbf{r}_2|} d\mathbf{r}_1 d\mathbf{r}_2. \tag{16}$$

2.2 Classical auto-correlation approach (FP)

Feingold and Peres [27] were the first to derive a semiclassical expression for matrix element variance in chaotic systems. There are two steps:

(i) relating off-diagonal variance a certain distance from the diagonal to the classical auto-correlation, then

(ii) relating diagonal variance to the off-diagonal variance close to the diagonal.

Step (i) has been more rigorously presented as a 'sum rule' for off-diagonal elements by Wilkinson who derived the result using a wavepacket approach [55]. Prosen [42] has extended the result to all types of classical dynamics. Moreover it has since been *proven* to hold asymptotically using microlocal analysis [57, 22], and in systems with a smooth potential using coherent states [23]. In the original FP paper step (ii) was argued, via the RMT expectation that (for a set of eigenfunctions in a small energy range) there is invariance under orthogonal basis rotations.

An alternative approach [25] for uniformly-hyperbolic systems uses a periodic orbit expansion and diagonal approximation, and enables the diagonal variance symmetry factor $g = 2$ to be justified at the periodic orbit level, thus avoiding the RMT assumption needed in step (ii). Hortikar and Srednicki [33] have also shown that if the free-space 2-point correlation (9) is replaced by its periodic orbit expansion, then the calculation of Section 2.1 becomes equivalent to step (i) of FP. Here we will perform step (i) using the QET, in a similar fashion to Cohen [19].

Step (i): We consider the 'signal' $A(t) := A(\mathbf{r}(t))$ as a function of time t for a given classical ergodic trajectory $\mathbf{r}(t)$ which starts at $(\mathbf{r}_0, \theta_0)$ in phase space at $t = 0$. Due to the scaling Hamiltonian for billiards we can choose unit speed, in which case t is arclength along the trajectory. The auto-correlation

of this signal is

$$C_A(\tau) := \lim_{T\to\infty} \frac{1}{T}\int_0^T A(t)A(t+\tau)\,dt \tag{17}$$

$$= \overline{A(0)A(\tau)} \tag{18}$$

where the ergodic theorem was used to rewrite the time average as an average over initial phase space locations. For any finite τ, the function $\mathcal{A}(\mathbf{r}_0, \theta_0) := A(0)A(\tau)$ is a smooth (although possibly convoluted) function of phase space $(\mathbf{r}_0, \theta_0)$. We will only need to consider τ of order t_{corr}, the system's correlation decay time. Applying QET[1] to the symbol $\mathcal{A}$ gives, for all n excluding a density-zero sequence,

$$\langle \phi_n, \hat{A}(0)\hat{A}(\tau)\phi_n\rangle \;\to\; C(\tau). \tag{19}$$

Here $\hat{A}(t)$ indicates the pseudodifferential operator corresponding to the classical symbol A, shifted in time by t (the usual Heisenberg picture in quantum mechanics). By considering the time-evolution of stationary states we express $\hat{A}(t)$ in the energy basis,

$$\langle \phi_n\, \hat{A}(t)\phi_m\rangle \;=\; A_{nm}e^{-i(k_m-k_n)t}. \tag{20}$$

The exponent involves wavenumbers because t measures arclength. (For simplicity we have chosen a dispersion relation $\omega = k$ in order to express unit wave group velocity; we are at liberty to choose any convenient dispersion relation). Inserting a complete set of states into (19) gives

$$\sum_{m=1}^{\infty} |A_{nm}|^2 e^{-i(k_m-k_n)\tau} \;\to\; C_A(\tau). \tag{21}$$

For row n of the matrix A_{nm}, we define the off-diagonal variance locally at a wavenumber 'distance' $\omega = k_m - k_n$ from the diagonal as

$$V_{A,n}(\omega) \;:=\; \Delta_k \sum_{m=1}^{\infty} |A_{nm}|^2 \delta_\epsilon(k_m - k_n - \omega), \tag{22}$$

where δ_ϵ is a smoothed delta function with width ϵ and unit mass. We scale ϵ in such a way that in the semiclassical limit an arbitrarily large number of

[1]Note that equivalently, Egorov's theorem can be used here to argue that the time evolution implicit in $A(0)A(\tau)$ does not invalidate QET

levels fall into the wavenumber range ϵ as $\epsilon \to 0$. For instance, $\epsilon \sim k^{-1/2}$. The mean level spacing expressed in terms of wavenumber is

$$\Delta_k \;=\; \frac{2\pi}{k\,\mathrm{vol}(\Omega)}, \tag{23}$$

as given by the leading Weyl law term. Taking the inverse Fourier transform of (22) then using (21) gives

$$\frac{1}{2\pi}\int e^{-i\omega\tau} V_{A,n}(\omega)\,d\omega \;\to\; \frac{\Delta_k}{2\pi} C_A(\tau). \tag{24}$$

This convergence is better expressed in the Fourier domain: using (23) we get

$$V_{A,n}(\omega) \;\to\; \frac{1}{k\,\mathrm{vol}(\Omega)}\tilde{C}_A(\omega) \tag{25}$$

where the power spectral density of the signal is

$$\tilde{C}_A(\omega) \;:=\; \int_{-\infty}^{\infty} C_A(\tau) e^{i\omega\tau} d\tau. \tag{26}$$

The power spectral density can be estimated from trajectory simulations (see Appendix A). Thus we have an asymptotic formula for off-diagonal variance of A_{nm} along all rows n excluding a density-zero sequence. If QUE were to hold then we would expect this exclusion to be lifted. This corresponds to a banded structure to the matrix A_{nm} (illustrated by Fig. 9), where the off-diagonal 'band profile' (local variance) is given by a classical power spectrum. Note that by using QET we have avoided the double energy-averaging of Wilkinson [55], instead arriving at an off-diagonal sum rule true for (almost all) individual rows of the matrix.

Step (ii): To approach the diagonal we take the limit $\omega \to 0$, which is well-defined because the exponential tails of $C_A(\tau)$ ensure that all of its moments are finite. To relate off-diagonal to diagonal variance the time-reversal invariance symmetry factor (14) was argued by FP to hold, again with $g = 2$, essentially by requiring invariance of the matrix element distributions under a basis rotation [27]. This can be justified by the idea, discussed in Section 2.1, that properties of eigenfunctions (within a narrow energy range) are invariant under basis rotations. Although this was not discussed by FP, the system must be assumed to be without further symmetry. It is crucial to note that if the system does possess other symmetries, then step (ii) can

break down altogether. Sarnak (Appendix 5 of [46]) has illustrated this for the case of a reflection symmetry: all diagonal matrix elements of an anti-symmetric A vanish (A only couples odd to even states), so diagonal variance is zero, therefore $g = 0$! Yet, the sum rule of step (i) would still hold in this case. Averaging (25) over a local range of n we have

$$V_A(E) \;=\; a_{\rm FP} E^{-1/2} \tag{27}$$

with prefactor

$$a_{\rm FP} \;=\; \frac{g}{\mathrm{vol}(\Omega)} \tilde{C}_A(0). \tag{28}$$

Finally, the physical significance of the correlation functions used above should be noted: the right-hand side of (25) is proportional to dissipation (heating) rate in a classical system driven at frequency ω with the forcing function A, and the left-hand side to quantum dissipation rate under equivalent forcing (with $\hat{A}$) within linear response theory (for reviews see [19, 9, 7]). Therefore (25) underlies another manifestation of the Correspondence Principle of quantum mechanics.

2.3 Existing numerical tests of FP

Now we review numerical tests of the FP prediction in chaotic systems. The validity of (25) was originally shown at the order-of-magnitude level in a double rotator model, a mixed finite-dimensional system [27]. The off-diagonal sum rule, step (i), has since been tested in a quartic oscillator, showing 50% or greater errors [3], in a limacon billiard (for mixed and fully ergodic cases), showing good (but unquantified) agreement over many orders of magnitude [42], and in the stadium billiard, with operators A comprising singular functions on the boundary (for which QET is not known to hold), showing agreement at the 10% level [8].

The diagonal variance has been shown to agree with FP to about 10% in the quantum Bakers map [25]. These researchers also studied the hydrogen atom in a strong magnetic field (nearly completely ergodic with sticky islands), and found some agreement at the 20% level, however they admit that the agreement was 'unexpectedly good' since it depended on a choice of smoothing parameter [25]. Better but unquantified agreement has since been found in this system for off-diagonal variance [17]. Tests of quantum ergodicity rate have also been performed which connect to FP. Notably, the

work of Bäcker *et al.* [5] has shown about 20% deviations from FP (see Errata for this work).

Common features of existing studies are: low and almost completely unquantified accuracy (*i.e.* lack of statistical rigor in the tests), and relatively low energy (quantum levels of order $n \sim 10^3$ to 10^4). In our work we remedy these omissions, by achieving tests of FP at known high accuracy, and at high energy.

3 Choice of system and numerical methods

We choose a generalized Sinai billiard with concave walls. Such everywhere-dispersing billiards are known [49] to be Anosov, and have been studied classically [9]. We consider a boundary formed from four circular arcs, with reflection symmetry about both x- and y-axes. We then desymmetrize (this reduces numerical effort for the quantum calculation [7]), to give Ω, the 'generalized quarter-Sinai billiard' shown in Fig. 1a. Because the two wall curvatures differ, there is no remaining symmetry, thus we believe the resulting billiard to be generic. Γ denotes the entire boundary of the (desymmetrized) billiard, and Γ_{desym} the part of Γ which excludes the symmetry lines (axes). We will study the odd-odd symmetry class only (Dirichlet boundary conditions on the axes, therefore on all of Γ). We choose the test function $A(\mathbf{r})$ piecewise constant in order to allow fast quantum calculation (Section 3.1). Throughout this work we use the function

$$A(\mathbf{r}) = \begin{cases} 1, & \mathbf{r} \in \Omega_A \\ 0, & \text{otherwise} \end{cases} \tag{29}$$

as shown in Fig. 1b, for which

$$\overline{A} \;=\; \frac{\mathrm{vol}(\Omega_A)}{\mathrm{vol}(\Omega)} \;\approx\; 0.55000 \tag{30}$$

and

$$A_{nm} \;:=\; \langle \phi_n, \hat{A}\phi_m \rangle \;=\; \langle \phi_n, \phi_m \rangle_{\Omega_A} \;:=\; \int_{\Omega_A} \phi_n(\mathbf{r})\phi_m(\mathbf{r})\, d\mathbf{r}. \tag{31}$$

Thus we have a 'chopped billiard' where the test function measures the mass lying on one side of the 'chop line'. Even though $A(\mathbf{r})$ is discontinuous the QET is known to apply [21]. Our choice of the shape of Ω_A was also informed

by the issue of boundary effects raised by Bäcker *et al.* [5] and discussed in Section 5.1.

Numerical calculations in our work separate into classical and quantum. The classical calculation of the power spectrum $\tilde{C}_A(\omega)$ is explained in Appendix A. The much trickier task of calculating the quantum matrix elements is discussed below.

3.1 Calculation of matrix elements

The numerical method used to find the Dirichlet eigenvalues $\{E_n\}$ and eigenfunctions $\{\phi_n\}$ is called the 'scaling method' [54]. It makes use of a basis set of size $N = O(N_{\rm sc})$, where the semiclassical basis size is

$$N_{\rm sc} := \frac{k|\Gamma_{\rm desym}|}{\pi}, \tag{32}$$

where $|\Gamma_{\rm desym}|$ indicates the (desymmetrized) perimeter. The method simultaneously returns the basis coefficients for the cluster of eigenfunctions whose eigenvalues lie within a narrow energy window. Per level this requires $O(N^2)$ numerical effort, which is faster by $O(N)$ than other known methods (summarized in [7]) such as boundary integral equations [6]. We have $N \approx 3500$ at the largest wavenumber reached ($k \approx 4000$) for the billiard under study; in this case the resulting efficiency gain is roughly a factor of 10^3! Similar efficiency gains have been reported in other studies of the Dirichlet eigenproblem at extremely high energy in both 2D [54, 53, 20, 18] and 3D [43]. Despite its success the scaling method has not yet been presented in a rigorous fashion (see [7] for a review). We refer the reader to the outline of the method presented in Appendix B, pending a more detailed account [11].

Once a large set of eigenfunctions (in the form of their basis coefficients) have been found, diagonal matrix elements are calculated using the following formula,

$$\langle u, v\rangle_{\Omega_A} = \frac{1}{2E} \oint_{\Gamma_A} (\mathbf{r}\cdot\mathbf{n})(Euv - \nabla u\cdot\nabla v) + (\mathbf{r}\cdot\nabla u)(\mathbf{n}\cdot\nabla v) + (\mathbf{r}\cdot\nabla v)(\mathbf{n}\cdot\nabla u)\, d\mathbf{s}, \tag{33}$$

where $\mathbf{s}$ is the boundary coordinate, $\mathbf{n}(\mathbf{s})$ is the outwards unit boundary normal vector, and $d\mathbf{s}$ is the line element on the boundary $\Gamma_A := \partial\Omega_A$. This identity holds for any two functions $u(\mathbf{r})$ and $v(\mathbf{r})$ which are regular solutions of the Helmholtz equation (1) at the same energy $E_u = E_v = E$

within an arbitrary bounded domain Ω_A. The functions u and v need satisfy no particular boundary conditions on Γ_A. The identity expresses an inner product over a domain purely in terms of boundary information. It is the $d = 2$ special case of an identity proved in the appendix of the companion paper [10] (see (36) in that paper), where the regularity conditions on u, v and Ω_A are also discussed. The diagonal matrix elements are found using (33) with $u = v = \phi_n$, and realising that the boundary integrand is nonzero only on $\Gamma_{A,\mathrm{desym}}$, the part of Γ_A excluding the symmetry lines.

Off-diagonal matrix elements are found via the more well-known identity,

$$\langle u, v \rangle_{\Omega_A} \;=\; \frac{1}{E_u - E_v} \oint_{\Gamma_A} (u\mathbf{n} \cdot \nabla v - v\mathbf{n} \cdot \nabla u)\, d\mathbf{s}, \tag{34}$$

which holds given the same conditions as for (33) except that $E_u \neq E_v$. (34) follows directly from Green's Theorem. Choosing $u = \phi_n$ and $v = \phi_m$, the boundary integrand is nonzero only on $\Gamma_{A,\mathrm{desym}} \setminus \Gamma$, that is, on the chop line. Thus by using (33) and (34), values and first derivatives of eigenfunctions on boundaries alone are sufficient to evaluate all matrix elements (31). The eigenfunctions need never be evaluated in the interior of Ω_A. For the boundary integrals, $O(N)$ quadrature points are needed, and at each point $O(N)$ basis evaluations are needed to calculate ϕ_n and its gradient, giving $O(N^2)$ effort per eigenfunction. This is $O(N)$ times faster than direct integration over Ω_A, an enormous efficiency gain.

Thus the eigenfunction calculation and the matrix element evaluation both scale as $O(N^2)$ per level. The calculations reported below took only a few CPU-days (1GHz Pentium III equivalent) in total. Most of the effort is spent evaluating basis (Bessel) functions and their gradients at the quadrature points.

4 Results

To give an idea of the typical energy range we work in, Fig. 2 shows a density plot of an eigenfunction at $E \approx 10^6$. Our calculations include data at energies 16 times greater than this, corresponding to $n \approx 7 \times 10^5$. Only a couple of studies in billiards have computed eigenfunctions at greater n, and they invariably involved shapes without corners (see for example [18]).

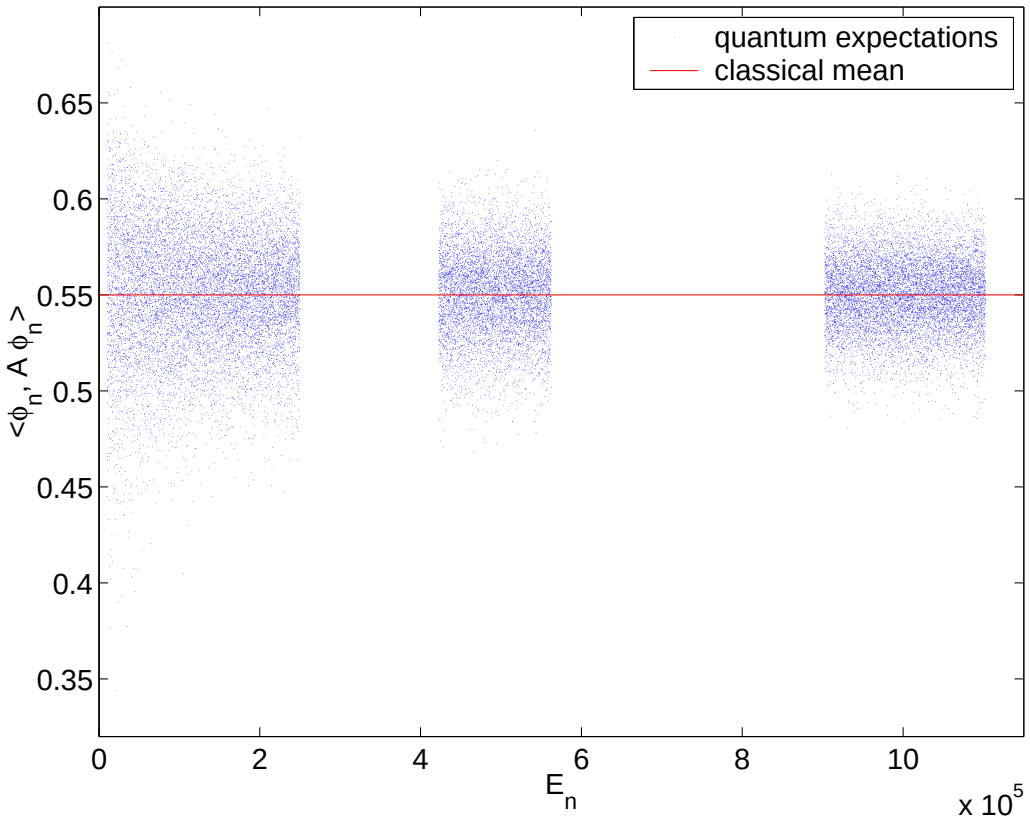

Figure 4: Scatter plot of diagonal matrix elements A_{nn} plotted against energy eigenvalue E_n. The gaps are due to the fact that only certain windows on the E axis have been computed; within each window all eigenvalues are found. The windows correspond to wavenumbers $k \in [100, 500]$, $k \in [650, 750]$ and $k \in [950, 1050]$, giving a total of 28171 levels. The classical mean $\overline{A}$ is shown as a horizontal line.

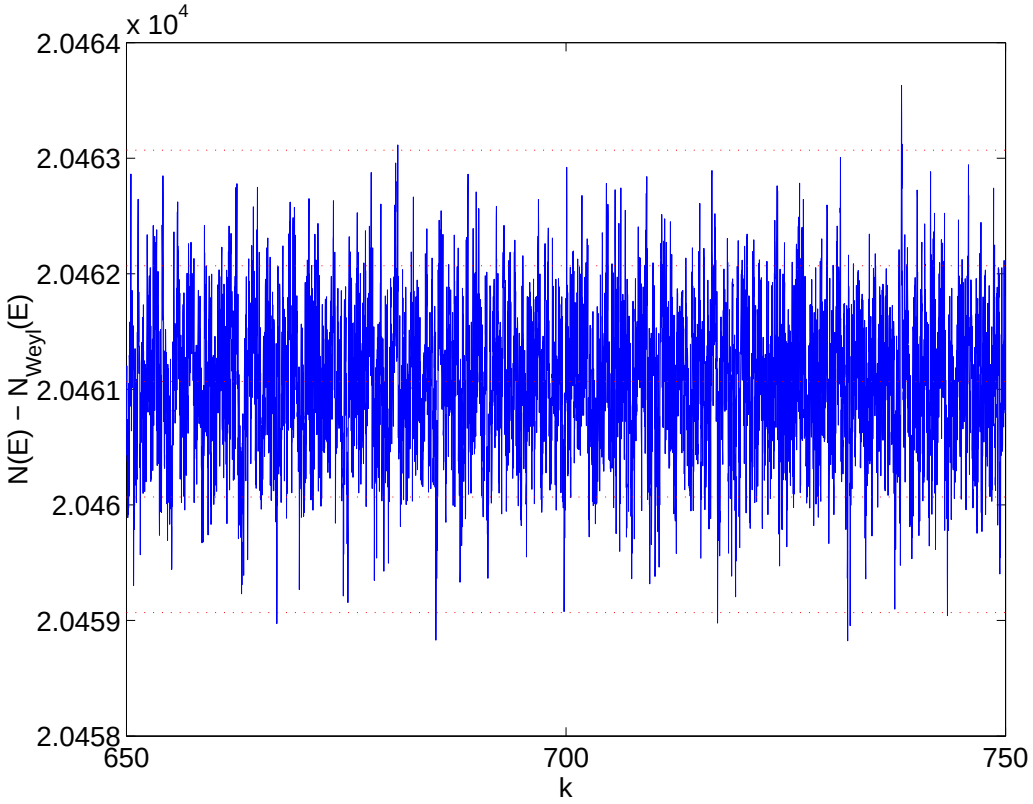

Figure 5: Demonstration that none of the 6812 levels are missing in the wavenumber window $k \in [650, 750]$. The level counting function $N(E) := \#\{n : E_n < E\}$ is plotted after the first two Weyl terms $N_{\mathrm{Weyl}}(E) = (\mathrm{vol}(\Omega)/4\pi)E - (|\Gamma|/4\pi)\sqrt{E}$ have been subtracted. The horizontal axis shows wavenumber $k = E^{1/2}$. Spectral rigidity ensures that a single missing or extra level can be detected [29]; this would be visible as a jump of size 1 (the gap between the dotted horizontal lines). No such jump occurs. Plots for the other two intervals in Fig. 4 look similar.

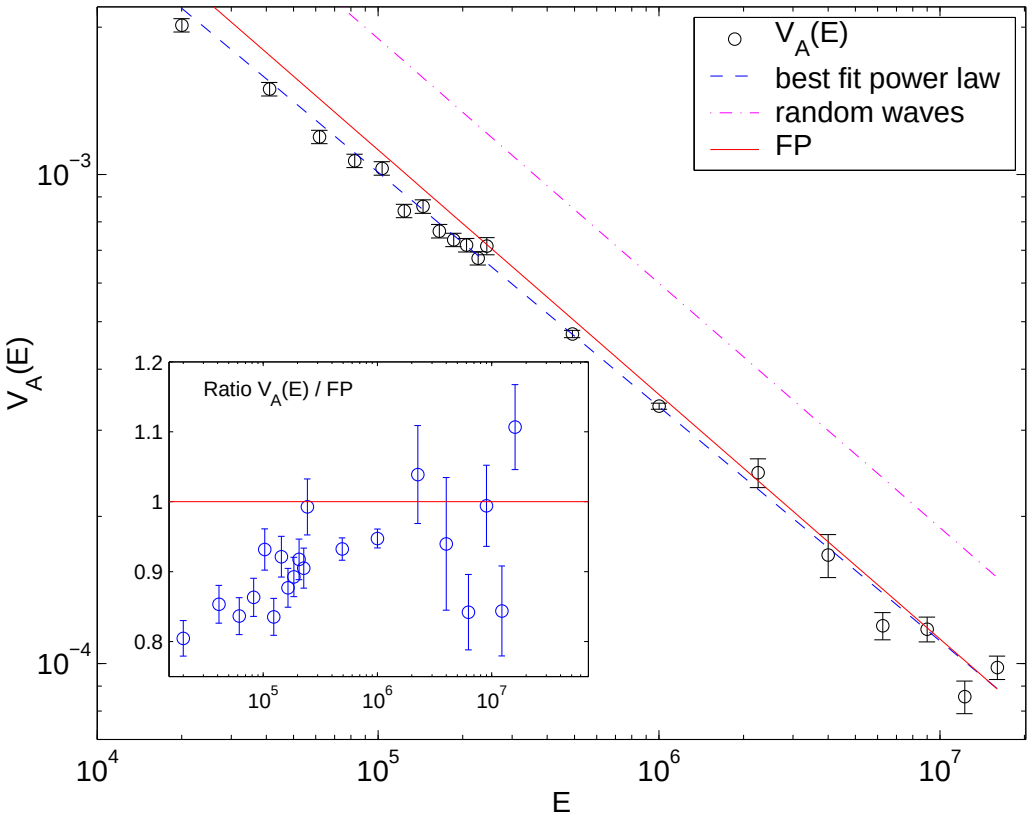

Figure 6: Variance of diagonal matrix elements A_{nn} as a function of energy E_n. $V_A(E)$ is plotted (with $\pm 1\sigma$ errorbars) for energy windows centered at the E values shown. The smallest errorbar is about 1.4% (at $E \approx 10^6$). The random wave prediction given by (15) and (16) has no fitted parameters (dash-dotted line). The FP semiclassical prediction given by (27) and (28) also has no fitted parameters (solid line). The best-fit power law $(\gamma_{\rm BF}, a_{\rm BF})$ is also shown (dashed line).

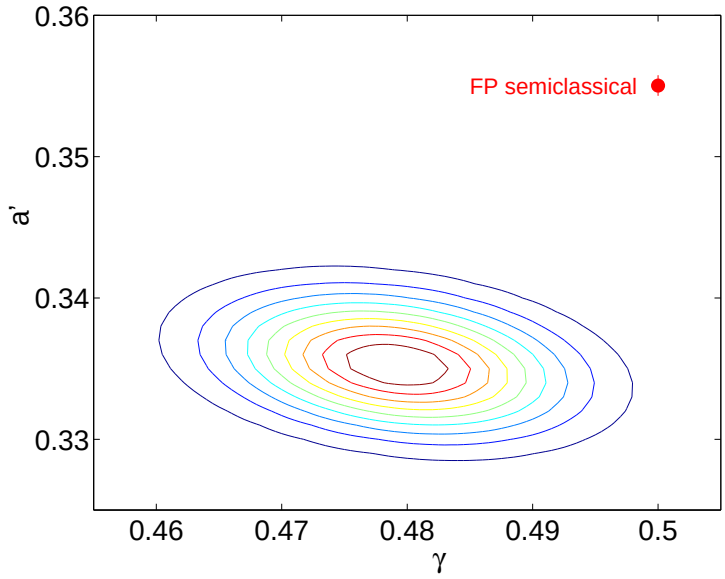

Figure 7: Comparison of power-law fit uncertainty with the FP semiclassical prediction. In the (γ, a') parameter plane, we show equally-spaced contours of the likelihood function, that is, likelihood that the data came from a power law model for the variance, with given parameters (γ, a'). See text for definition of a'. The FP prediction is shown as a large dot with an errorbar due to the classical power spectrum estimation.

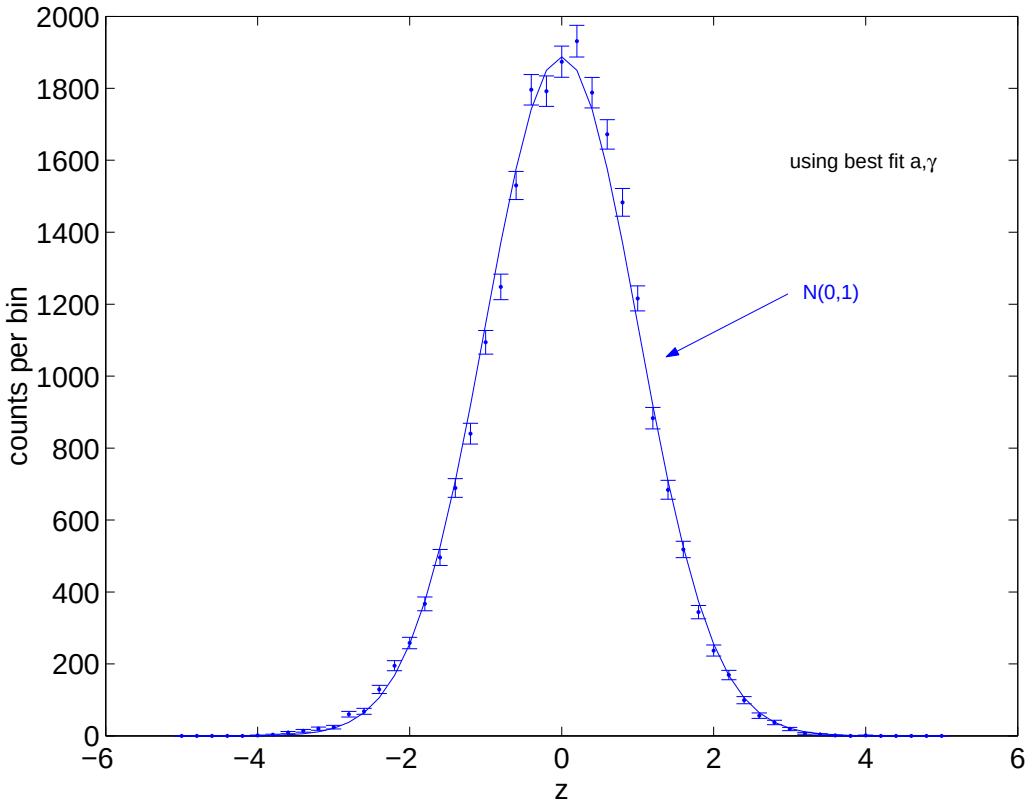

Figure 8: Histogram of rescaled deviations $z_n := (A_{nn} - \overline{A})/V_A(E_n)^{1/2}$, using the best-fit power law form (35), compared against an appropriately-normalized Gaussian distribution of unit variance.

	Best-fit $a_{\rm BF}^{(1/2)}$	Random wave $a_{\rm RW}$	Feingold-Peres $a_{\rm FP}$
prefactor	0.334 ± 0.003	0.5995 ± 0.001	0.3550 ± 0.0004
deviation from $a_{\rm BF}^{(1/2)}$	—	$79 \pm 1\%$	$6.5 \pm 0.9\%$

Table 1: Comparison of measured (best-fit) prefactor to the two semiclassical prefactor estimates assuming $\gamma = 1/2$ power-law decay of quantum variance with energy. The random wave estimate is (16) and the Feingold-Peres is (28).

4.1 Evidence for Quantum Unique Ergodicity

Fig. 4 shows values of diagonal matrix elements A_{nn}, for all E_n lying in certain energy windows, up to about $E \approx 10^6$, comprising 28171 levels. We are certain that all quantum levels and no duplicates have been found in the energy ranges shown: for instance the comparison of the level counting function against Weyl's law in Fig. 5 shows not a single missing or duplicate level. We continued collecting smaller windows at higher energies up to $E \approx 1.6 \times 10^7$, comprising another 2718 levels (calculation is more time-consuming at higher energy). The slow decay of the size of deviations from the classical mean can be seen in Fig. 4.

Are the quantum expectations condensing to the classical mean? We find that the average of A_{nn} at low energies is slightly, but detectably, higher than $\overline{A}$. However, if we restrict ourselves to $E > 9 \times 10^4$, the mean of these 27037 levels is 0.55023 ± 0.00013, where the error quoted is $\pm 1\sigma$ (standard deviation). This is about 1.8σ from the classical mean (30), thus our data is consistent with convergence to the classical mean with a relative error of 0.02%.

Of this entire collection, both the maximum 0.6811 and minimum 0.3437 of A_{nn} occur at $E_n < 2 \times 10^4$, visible at the far left side of Fig. 4. Furthermore there is not a single exceptional value falling outside of this slowly-condensing distribution. If there is a sequence of strongly-scarred states (where the form of the scarring gives an anomalous value of A_{nn}), this implies that its density is unlikely to be more than 3×10^{-5}. This provides strong support for the QUE conjecture in this system.

4.2 Ergodicity rate

At what rate are the quantum expectations tending towards the classical mean? We measure variance $V_A(E)$ for levels within local windows of energy, to give the data with errorbars shown in Fig. 6. The relative errorbar of an estimator of variance is $\sqrt{2/N}$ if N independent samples from a Gaussian population are taken. For instance, we would need to collect 20000 samples in order to achieve a 1% errorbar—this explains why previous studies have not achieved high accuracy. We perform a (correctly statistically weighted) fit of the parameters (γ, a) in a power-law model,

$$V_A(E) \;=\; aE^{-\gamma}. \tag{35}$$

We found that restricting to data with $E > E_{\min} = 1.6 \times 10^5$ was needed to avoid corruption by the non-asymptotic dependence at lower energy (fitted values were dependent on $E_{\min}$ when $E_{\min}$ was set any lower). However, because of the slow convergence, we still cannot be sure that we have reached the asymptotic regime. The best-fit value of γ was found to be

$$\gamma_{\rm BF} \;=\; 0.479 \pm 0.009. \tag{36}$$

This is very close (but a 2.3σ deviation) to the $\gamma = 1/2$ power expected from both semiclassical estimates in Section 2. The errorbar here was found from the width of the likelihood function when marginalized over a. (Recall that the likelihood, as a function of model parameters, gives the likelihood that the data came from a model with those parameters [50]). This best-fit power law $(\gamma_{\rm BF}, a_{\rm BF})$ is shown in Fig. 6. The distribution of rescaled deviations, given this power law, is shown to be very close to Gaussian in Fig. 8.

We now consider the question: assuming the semiclassical power law $\gamma = 1/2$ is in fact correct, how well does the prefactor match the estimates from Section 2? Fixing $\gamma = 1/2$, we fit for the prefactor a to get $a_{\rm BF}^{(1/2)}$, and compare against semiclassically predicted values, in Table 1. The random wave prefactor overestimates by nearly a factor of two: this is hardly surprising since the support of $A(\mathbf{r})$ covers an $O(1)$ fraction of the total volume, and extends to the boundary of Ω where the random wave assumption surely breaks down (no reflected waves have been taken into account). By careful consideration of the errorbars, we see that the deviation between fitted $a_{\rm BF}^{(1/2)}$ and the FP prediction $a_{\rm FP}$ (28) is statistically significant: FP overestimates by about 7σ. The systematic deviation is visible at low and intermediate

energies in the inset of Fig. 6; at high energies the errorbars are sufficiently large that there is no evidence for systematic deviation.

In order to visualize where FP falls relative to the statistical uncertainty in the power law fit, in Fig. 7 we plot the likelihood over the (γ, a') parameter space given the quantum variance data. For this plot we used an equivalent version of (35),

$$V_A(E) = a' E_0^{-1/2} \left(\frac{E}{E_0} \right)^{-\gamma}, \tag{37}$$

with the 'pivot' energy is $E_0 = 10^6$, for the simple reason that with this choice γ and a' are nearly uncorrelated, aiding the visual interpretation (cf. γ and a are highly correlated). Note that when $\gamma = 1/2$, $a' = a$. In this plot the FP prediction $(1/2, a_{\rm FP})$ is shown for comparison. If FP exactly explained the variance data, we would expect the dot to fall within the likelihood probability 'blob'; the fact that it doesn't indicates statistically significant deviations.

4.3 Off-diagonal variance (band-profile)

By computing off-diagonal matrix elements we can test step (i) of FP directly. The amount of data we can collect for any single matrix row n is insufficient to estimate $V_{A,n}(\omega)$ to any useful accuracy. Therefore we measure a local energy average of this quantity,

$$V_A(E, \omega) \; := \; \frac{1}{M} \sum_{E_n \approx E}^{N \le n < N+M} V_{A,n}(\omega), \tag{38}$$

to which we expect $V_{A,n}(\omega)$ to converge for all levels n barring a vanishing-density set. As with (8), a large number of levels M needs to be chosen which span an energy range much smaller than E itself (this can be much larger than the averaging scale $\epsilon \to 0$ implicit in $V_{A,n}(\omega)$ required to converge the off-diagonal structure). $V_A(E, \omega)$, equivalent to Wilkinson's $S(E, \Delta E)$ [55], measures the off-diagonal band profile (variance) of the matrix A_{nm}, by averaging over an oblique, narrow 'patch' of the matrix. A density plot of a piece of this matrix is shown in Fig. 9.

Fig. 10 shows $V_A(E, \omega)$ estimated around $E = 4.9 \times 10^5$, compared to FP, that is, the classical power spectrum (25). About 2.3×10^6 distinct matrix elements were calculated between 6812 eigenfunctions. There are no fitted

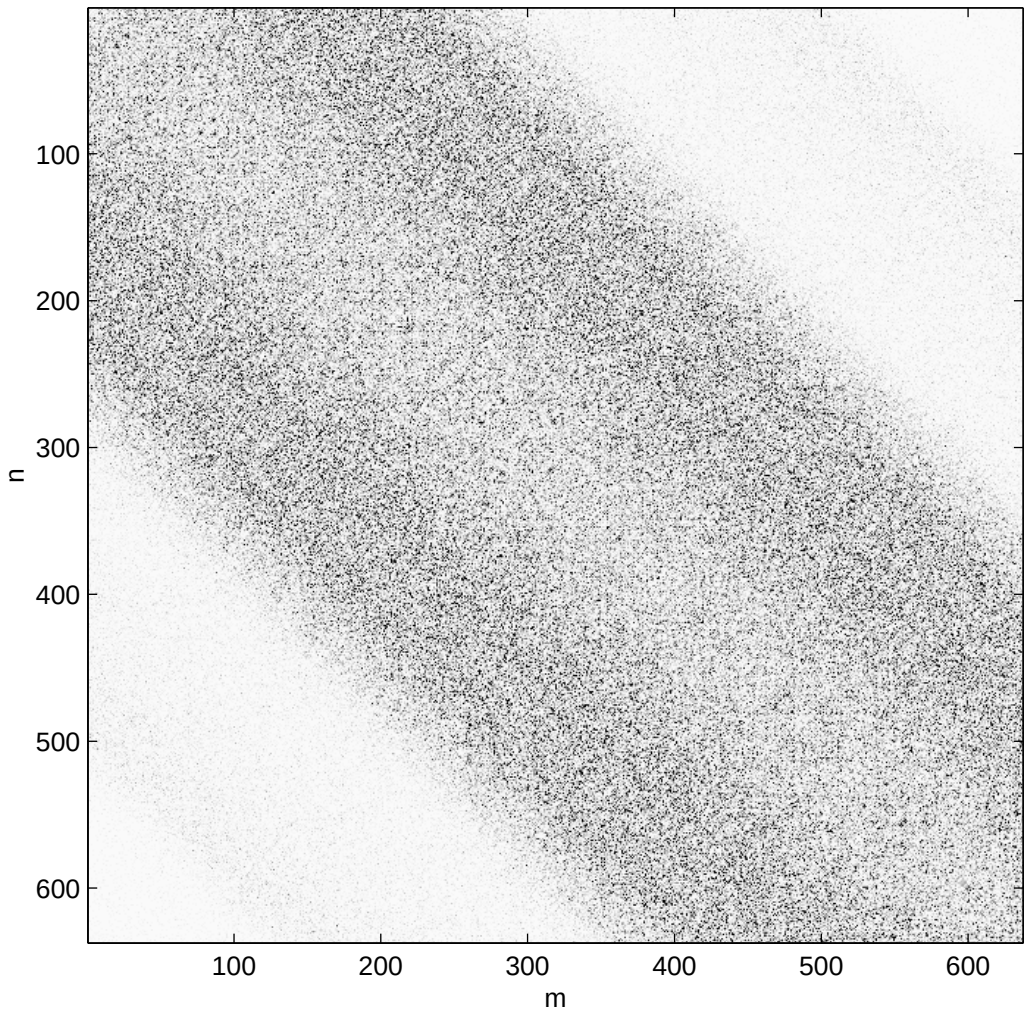

Figure 9: Density plot of squared matrix element deviations $|A_{nm} - \delta_{nm}\overline{A}|^2$ for the 637 quantum levels lying in $k \in [650, 660]$, shown in the form of the matrix. The range white to black indicates zero to 1.7×10^{-3}. The band profile (ω-dependent variance, see Fig. 10) appears to be the only significant structure, other than the matrix being symmetric.

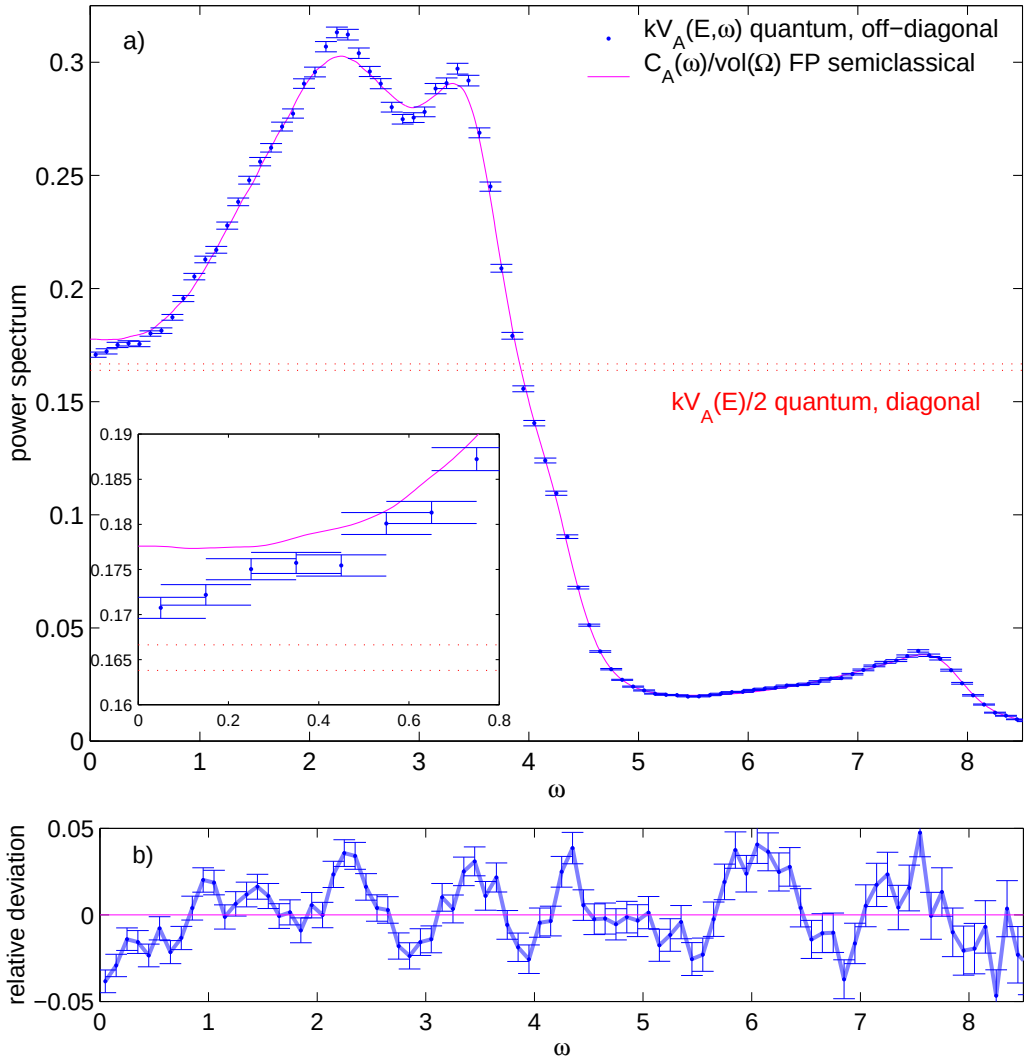

Figure 10: a) Average quantum variance $V_A(E;\omega)$ (errorbars) as a function of distance ω (wavenumber units) from the diagonal, compared against FP (25) (solid line). Errorbars are 0.7% for quantum (near the diagonal), 0.2% for classical. Half the diagonal variance is shown as two horizontal dotted lines indicating ± 1 standard deviation. Matrix elements between the 6812 eigenfunctions with $k_n \in [650, 750]$ were used to generate the quantum data, by rescaling (assuming $\gamma = 1/2$) appropriately to $k = 700$. Inset is a zoom on the $\omega \to 0$ region. b) Relative deviation between quantum variance and FP.

parameters. The agreement is excellent. With 0.7% quantum errorbars (near the diagonal) this is believed to be the most accurate test of the Feingold-Peres result ever performed. However it is clear (Fig. 10b) that there is statistically significant deviation: the peaks and valleys (points of highest curvature) are exaggerated more in the quantum variance than the classical power spectrum, by up to about 3% (4σ). This is a real effect: the smoothing of $\tilde{C}_A(\omega)$ (see Appendix A) is on a much finer ω scale and cannot explain the rounding of the peaks and valleys. The situation at $\omega = 0$ could be viewed as another example of this (the power spectrum being a symmetric function of ω). The deviation between FP and the observed $\omega \to 0$ limit of $V_A(E, \omega)$ is $3.8 \pm 0.7\%$.

The diagonal quantum variance, divided by $g = 2$, is also shown. If step (ii) of FP applied exactly then this would coincide with $V_A(E, 0)$, however a $3 \pm 1\%$ difference is found. It is unlikely but possible that this is merely a statistical fluctuation (a null result). Thus, at this energy, the diagonal variance prefactor discrepancy of 7% seems to result from the addition of two roughly equal effects: step (i) has about 4% discrepancy, and step (ii) about 3%.

5 Discussion

We return to our chief issue: quantum ergodicity, as measured by diagonal variance. Looking at Fig. 6, we could postulate three hypotheses for the variance $V_A(E)$:

I. There is asymptotic agreement with FP, $\gamma = 1/2$ with prefactor a_{FP} given by (28), but the convergence to this is quite slow.

II. There is power-law behaviour with the power being the semiclassically expected $\gamma = 1/2$, but the prefactor differs, $a \neq a_{\mathrm{FP}}$. Again, we admit the possibility of slow convergence here.

III. There is power-law behaviour but with a new power $\gamma \neq 1/2$ (therefore the prefactor cannot be related to semiclassical estimates).

Our data is consistent with hypothesis I, if for example we assume a finite-E correction of the form

$$V_A(E) \approx a_{\mathrm{BF}} E^{-1/2} \left(1 - bE^{-\beta} + o(E^{-\beta})\right) \tag{39}$$

with β sufficiently small, and b sufficiently large. We do not have enough data to do a meaningful fit for β and b, however, our data suggests $0.25 \leq \beta \leq 0.5$, and that b is several times greater than 1. On the theoretical side, the issue of finite-E (finite-$\hbar$) corrections to FP appears unresolved: the $O(\hbar)$, here corresponding to $O(E^{-1/2})$, periodic orbit corrections derived by Wilkinson [55] were later claimed by Prosen not to contribute at this order [42]. Thus future analytic and numerical study is needed in this area. Our data imply that asymptotic convergence is very slow, and that we would have to collect a lot of statistics at $E \sim 10^7$ or above to improve upon the 6–7% variance discrepancy found at $E \sim 10^6$ (where the bulk of our data was taken). This slow convergence is best shown in the inset of Fig. 6.

Our data is equally well consistent with hypothesis II, but only if we also allow slow convergence here. The observed slope in our energy range being shallower than $\gamma = 1/2$ indicates that, asymptotically, the prefactor deviation would be less than 6.5%. Differences in prefactor have actually been recently *proved* to hold in arithmetic systems [46, 37]. As a function of the operator A, both quantum (diagonal) variance and classical variance (the FP prediction) are quadratic forms. In the arithmetic setting these quadratic forms are remarkably diagonalized (asymptotically) by the ϕ_n themselves, but with differing corresponding eigenvalues. This would correspond to the presence of an A-dependent prefactor in (27), (28). It would be fascinating if this carried over to our Euclidean billiard case.

Our data is consistent with hypothesis III, with the power given by (36). However there is not enough data to distinguish between I and III (this would require more statistics, *e.g.* another 10000 eigenfunctions at $E \sim 10^7$).

The off-diagonal variance data in Section 4.3 offers us the insight that at $E \approx 4.9 \times 10^5$, the off-diagonal band profile is very close to, but has not yet converged to, the FP prediction. Convergence is ω-dependent, and, as with the diagonal, seems very slow. However, as discussed in Section 2.2, asymptotically step (i) of FP is proven to hold. So if hypothesis II holds, then step (ii) alone must account for the prefactor discrepancy, that is, $g \neq 2$. In our case, g would tend to about 1.85. Any such deviation from the RMT (GOE) value $g = 2$ would be surprising, since it tells us that there are significant (in this case positive) correlations between eigenfunctions with nearby n. Instead if hypothesis III held, g would have to tend to 0 (for $\gamma < 1/2$) or ∞ (for $\gamma > 1/2$), both unsettling prospects for a system which does not possess remaining symmetries. As is stands, our data only shows a 3σ discrepancy from $g = 2$, which is not tremendously significant. So if

hypothesis I holds, it may be that in fact $g = 2$, leaving all the discrepancy in the diagonal case to be accounted for by the slow convergence of step (i). We note that, for the uniformly-hyperbolic case, any hypothesis other than I would be inconsistent with the derivation of Eckhardt *et al.* [25].

Recently Zelditch [59] has shown that QUE, if valid, extends to off-diagonal matrix elements. We find strong numerical evidence for off-diagonal QUE: there are no exceptionally large off-diagonal elements in data such as Fig. 9.

Can our observed rate of ergodicity be reconciled with scar theory? As now understood, scar theory [39] predicts typical intensity enhancements along each UPO staying constant (*not* vanishing) as $E \to \infty$. However, the width of the scarred region transverse to the UPO scales like $E^{-1/4}$ (in 2D), so *does* vanish, and along with it the amount of excess probability mass associated with the scar. Scar-related fluctuations in A_{nn} would then die like $E^{-1/4}$, corresponding to the FP power law $\gamma = 1/2$. Therefore there is no conflict.

It is worth comparing our results to the previous numerical work on quantum ergodicity in billiards. Aurich and Taglieber tested polygons in the hyperbolic plane, and found rough agreement with $\gamma = 1/2$ [2]. The only known study on Euclidean billiards, that of Bäcker *et al.* [5], contains exhaustive permutations of billiard and Ω_A region shapes, but was limited to $n < 6000$. They found assorted power laws, covering the range $\gamma = 0.37$ to 0.5 even for the (Anosov) cardioid billiard. If our hypothesis I is to be believed, the slow asymptotic convergence of variance we find explains why their power laws are so at odds with expectation, and why when they are close to $\gamma = 1/2$, the prefactors differ from FP by 20% (see Errata to [5]). By reaching 100 times higher in E, we can see (Fig. 6) that the apparent power law for low energies ($E < 10^5$) is deceptive (non-asymptotic). Their study, by focussing on a sum $S_1(E, A)$ over *all* levels up to n, also integrated away useful information on individual eigenfunction variances and resulted in less conclusive results, of unquantified statistical significance.

5.1 Effect of Gibbs phenomenon at the boundary

In this section we estimate if boundary effects could be responsible for the observed difference between quantum variance $V_A(E)$ and FP. The Dirichlet boundary condition means that very close to the walls the eigenfunction intensity must vanish. The result is an oscillation or 'ringing' (Gibbs phe-

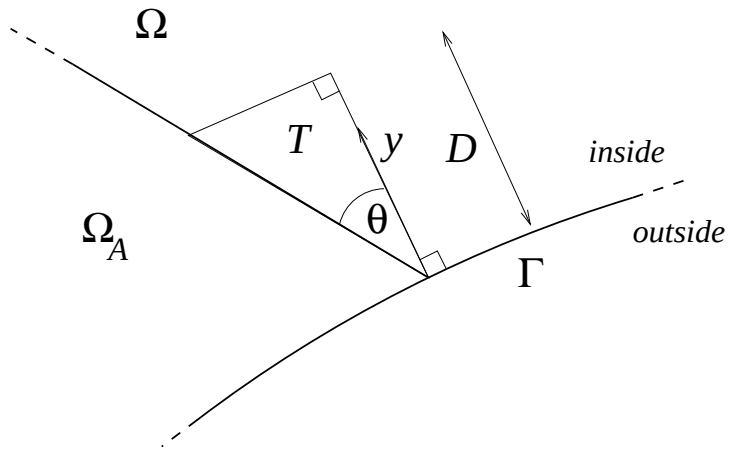

Figure 11: Geometry for estimating the effect of oscillations in mean eigenfunction intensity near the wall.

nomenon) in the mean intensity $|\phi_n|^2$ as a function of $d(\mathbf{r})$, the shortest distance from point $\mathbf{r}$ to the boundary, namely

$$\langle|\phi(\mathbf{r})|^2\rangle = \frac{1}{\mathrm{vol}(\Omega)}\left(1 - J_0(2kd(\mathbf{r})) + O(\frac{1}{kL})\right) \tag{40}$$

The oscillation occurs at distance scale $1/k_n$ and dies like square root of distance. The symbol $\langle\cdot\rangle$ means a local energy average (an average over eigenfunctions ϕ_n whose wavenumbers k_n are very close to k). The $O(1/kL)$ correction is due to the perimeter term in the Weyl level density. The functional form has been proved analytically for $\Gamma \in C^\infty$ [32] and it has been verified numerically [5] that this is the dominant correction to the uniformity of $|\phi|^2$ in billiards. It can most simply be derived by considering that the random wave assumption must be modified near a (straight) boundary by addition of a reflected wave in order to preserve the boundary condition, then making use of (9).

As pointed out by Bäcker this effect causes the quantum mean expectation value to differ from $\overline{A}$, for any finite E. How significant are its effects on our study, and could it explain any discrepancies in variance? We can estimate $\Delta\mu$, the deviation of mean A_{nn} from the classical average $\overline{A}$, using the integral

of (40) inside the triangle T (of height D) shown in Fig. 11,

$$\begin{aligned}\Delta\mu &\approx \frac{\int_T (1 - J_0(2ky))\, d\mathbf{r} - \mathrm{vol}(T)}{\mathrm{vol}(\Omega)} \\ &\approx -\frac{1}{\mathrm{vol}(\Omega)} \int_0^D J_0(2ky) y \tan\theta \, dy \\ &= -\frac{D\tan\theta}{2\mathrm{vol}(\Omega)} \frac{J_0(2kD)}{k}. \end{aligned} \tag{41}$$

Here we assumed that distances are small compared to radius of curvature, in which case $d(\mathbf{r}) \approx y$. In an infinite sized system the limit $D \to \infty$ could now be taken, in which case (41) diverges at any fixed k. However in any finite sized billiard Eq. (40) and our form for $d(\mathbf{r})$ will break down for distances D comparable to the billiard size L. This will destroy the coherent addition which causes the divergence, and allows us to fix D at a constant of order L. For $kD \gg 1$ the asymptotic form of the Bessel function then gives the bound $|\Delta\mu| < cE^{-3/4}$ where c contains geometric constants.

To see if this systematic shift in mean is significant, it should be compared to the quantum deviations. The bound on $\Delta\mu$ is $O(E^{1/2})$ smaller than the deviation size $\sim E^{-1/4}$, meaning that it will have an insignificant effect on variance at the energies studied. Indeed this is supported by the highly accurate mean agreement found in Section 4.1. To conclude, boundary effects cannot explain the observed discrepancies of several %.

Finally a word on the choice of domain Ω_A is in order. We avoided the use of an interior domain (where $\Gamma \cap \Gamma_A = \{0\}$) not only to minimize the perimeter $\Gamma_A \setminus \Gamma$ on which (33) need be evaluated, but to reduce sensitivity to the above ringing effect. Bäcker *et al.* investigated domains with boundaries containing long segments parallel and close to Γ, and as they point out, these were therefore very sensitive to the ringing effect [5]. Using this knowledge, we were able to avoid such choices.

6 Conclusions

We have studied a generic Euclidean Dirichlet billiard whose classical dynamics is Anosov, testing quantum ergodicity by comparing quantum expectations (diagonal matrix elements) A_{nn} to the classical mean $\overline{A}$ for a piecewise-constant position-dependent operator A. For over 30000 computed

eigenfunctions ϕ_n, no values of A_{nn} were found to fall outside of a Gaussian distribution which slowly condenses around $\overline{A}$. This is strong evidence for Quantum Unique Ergodicity. The ergodicity rate is quantified by $\mathrm{var}(A_{nn})$ (quantum variance). Calculating this numerically up to unprecedented energies (100 times higher n than any previous ergodicity study) and with unprecedented accuracy (due to the large number of eigenfunctions computed), diagonal variance is found to obey a power law (35) remarkably well over 3 decades of energy (Fig. 6). Such large-scale high-energy matrix element calculations would not be possible without the scaling method (a factor of 10^3 faster than other boundary methods) with a new basis set introduced by the author (Appendix B), and the identity (33) which allows diagonal matrix elements to be evaluated using boundary integrals alone.

The variance power law was found to deviate by only 4% from the semiclassically predicted $\gamma = 1/2$ (which we note is also consistent with scar theory). If $\gamma = 1/2$ is assumed to hold asymptotically as $E \to \infty$, then convergence to this law is surprisingly slow. As a result, even at the high energies we test (the bulk of data coming from $E \approx 10^6$, or $n \approx 5 \times 10^4$), we cannot tell if the observed 7% variance deviation from the Feingold-Peres prediction (27) and (28) will vanish (hypothesis I) or persist (hypothesis II) asymptotically. This distinction is important to resolve since in arithmetic systems a persistent prefactor difference has recently been proven analytically [46, 37]. The slow convergence helps explain the fluctuating γ observed in a previous ergodicity study at much lower E [5]. Neither can we rule out a persisitent power law of $\gamma = 0.48 \pm 0.01$ (hypothesis III). However the effect of known eigenfunction boundary effects has been estimated and ruled out as a possible cause for the observed deviation. More data at higher E would be needed to resolve the matter; given the numerical tools presented here this is simply a matter of increased CPU time.

We have also tested the FP prediction, step (i), that off-diagonal matrix element variance has a banded off-diagonal profile given by the classical power spectrum, at an unprecedented 0.7% accuracy level at around $n \approx 2.5 \times 10^4$. We find excellent agreement, but that systematic ω-dependent discrepancies of up to 4% exist, for which no theory yet exists. Given that off-diagonal variance is proven to obey FP asymptotically, we can only assume this is another manifestation of slow convergence. The observed 3% discrepancy in the RMT (GOE) predicted symmetry factor $g = 2$, that is, step (ii) of FP, is a surprise, but is not statistically highly significant. Our data strongly support a QUE conjecture for off-diagonal matrix elements.

Clearly, in order to perform this first large-scale study, we have limited ourselves to one billiard Ω and one operator A. In order to complete the picture, the rate of ergodicity, more precisely the deviations from the FP prediction for the rate, should be studied as a function of Ω and A. If indeed hypothesis I does then prevail, then an understanding of the corrections such as b and β in (39) becomes a priority.

Acknowledgements

This work was inspired by questions of Peter Sarnak, with whom the author has had important and enlightening interactions. We have also benefitted from discussions with and feedback from Percy Deift, Fanghua Lin, Eduardo Vergini, Doron Cohen, Eric Heller and Kevin Lin. The author is supported by the Courant Institute at New York University.

Appendix A: Classical power spectrum

$\tilde{C}_A(\omega)$ defined by (26) is the Fourier transform of the auto-correlation of observable A, and is otherwise known as the spectral density. We will use standard techniques to estimate it [28]. For a particular trajectory, launched with certain initial location in phase space, $A(t)$ is a noisy function (stochastic stationary process). We define its windowed Fourier transform as

$$\tilde{A}(\omega) \ := \ \int_0^T A(t) e^{i\omega t} dt, \tag{42}$$

where the window is a 'top-hat' function from 0 to T. Using with (17) and (26), and taking care with order of limits, we have the Wiener-Khinchin Theorem,

$$\tilde{C}_A(\omega) \ = \ \lim_{T\to\infty} \frac{1}{2\pi T} \, \tilde{A}^*(\omega)\tilde{A}(\omega). \tag{43}$$

For this single trajectory, $\tilde{A}(\omega)$ is a rapidly-fluctuating random function of ω, with zero mean (for $\omega \neq 0$), variance given by $2\pi T \tilde{C}_A(\omega)$, and correlation length in ω of order $2\pi/T$. (As $T \to \infty$, the ω-correlation becomes a delta-function). Thus (43) converges only in the weak sense, that is, when smoothed in ω by a finite width test function.

A given trajectory is found by solving the particle collisions with the straight and circular sections of Γ, and $A(t)$ is sampled at intervals $\Delta t = 0.02$ along the trajectory (recall we assume the particle has unit speed). Then $\tilde{A}(\omega)$ is estimated using the Discrete Fourier Transform (DFT, implemented by the FFT) of this sequence of samples, giving samples of the spectrum at ω values separated by $\Delta\omega = 2\pi/T$. The correlation in ω is such that each sample is (nearly) independent. Δt was chosen sufficiently short that aliasing (reflection of high-frequency components into apparently low frequencies) was insignificant. A trajectory length $T = 10^4$ (about 1.8×10^4 collisions) was used. The finiteness of T causes relative errors of order $t_{\rm corr}/T$, where $t_{\rm corr} \approx 2$ (for our domain) is the timescale for exponential (since the billiard is Anosov) decay of correlations. Thus more sophisticated window functions are not needed.

Given $\tilde{A}(\omega)$ we use (43), with the fixed T, to estimate $\tilde{C}_A(\omega)$. We smooth in ω by a Gaussian of width $\omega_{\rm sm} = 0.03$. This width is chosen to be as large as possible to average the largest number of independent samples from the neighborhood of each ω, but small enough to cause negligible convolution of the sharpest features of $\tilde{C}_A(\omega)$.

Finally, in order to reduce further the random fluctuations in the estimate, $n_r = 6000$ independent trajectory realizations with random initial phase space locations were averaged. An estimate for the resultant relative error ϵ in $\tilde{C}_A(\omega)$ can be made by counting the number N of independent random samples which get averaged, and using the fact that the variance of the square of a Gaussian zero-mean random variable (*i.e.* χ^2 distribution with 1 degree of freedom) is twice the mean. This gives

$$\epsilon \;=\; \left(\frac{2}{N}\right)^{1/2} \;\approx\; \left(\frac{2\pi}{n_r \omega_{\rm sm} T}\right)^{1/2}, \tag{44}$$

which numerically has been found to be a conservative estimate. In our case $\epsilon \approx 2 \times 10^{-3}$, that is, about 0.2% error.

The zero-frequency limit $\tilde{C}_A(0)$ is found using the smoothed $\tilde{C}_A(\omega)$ graph at $\omega = 0$, and therefore is an average of frequencies within $\sim \omega_{\rm sm}$ of zero. This approach is justified because exponential correlation decay results in all moments of $C_A(\tau)$ finite, hence there is no singularity in $\tilde{C}_A(\omega)$ at $\omega = 0$ (it can be expanded in an even Taylor series about $\omega = 0$ with finite coefficients).

Appendix B: Scaling method for the Dirichlet eigenproblem

The 'scaling method' for the solution of the Dirichlet eigenproblem in star-shaped domains was invented by Vergini and Saraceno [54], and considering its great efficiency (discussed above in Section 3.1) it has received remarkably little attention. Here we give only an outline.

Let Ω be a bounded Euclidean domain in $\mathbb{R}^d$, with $d \geq 2$. For example we envisage a domain with boundary composed of a finite number of piecewise smooth surfaces. Let $\Gamma := \partial\Omega$ be the boundary parametrized by the $(d-1)$ dimensional coordinate $\mathbf{s} \in \Gamma$, with outwards unit normal vector $\mathbf{n}(\mathbf{s})$. Dirichlet eigenfunctions are defined by (1) with (2). The method relies on the remarkable fact that the normal derivatives of eigenfunctions lying close in energy are 'quasi-orthogonal' (nearly orthogonal) on the boundary, with respect to the boundary weight function $r_n := \mathbf{r} \cdot \mathbf{n}$, where $\mathbf{r}$ is the position vector relative to some origin. This can be expressed by the identity,

$$Q_{ij} := \oint_\Gamma r_n (\mathbf{n} \cdot \nabla\phi_i)(\mathbf{n} \cdot \nabla\phi_j)\, d\mathbf{s} \;=\; 2E_i\delta_{ij} + \frac{(E_i - E_j)^2}{4}\langle \phi_i, r^2\phi_j\rangle_\Omega, \quad (45)$$

where $d\mathbf{s}$ is the surface element. The content of (45) is that, since r^2 is a bounded operator on the domain, off-diagonal elements of Q must vanish quadratically as one approaches the diagonal. Thus the matrix $Q_{ij}/2E_i$ approximates the identity matrix, when restricted to an energy window $E_i, E_j \in [E - \epsilon_0, E + \epsilon_0]$, if the window size remains relatively narrow $\epsilon_0 = o(E^{1/2})$. The proof of (45), and its generalization to adjoint boundary conditions, is presented in [10] (where it is Lemma 1.1).

We choose a 'center' wavenumber $k = E^{1/2}$, near which we are interested in extracting eigenfunctions, and relative to which the wavenumber shift of level i is $\omega_i(k) := k - k_i$. Consider an eigenfunction ϕ_i for which $\omega_i < 0$ and $|\omega_i| \ll O(1)$. We create a version spatially rescaled (dilated about the origin) by an amount needed to bring its wavenumber to k, that is, $\chi_i(k, \mathbf{r}) := \phi_i(k\mathbf{r}/k_i)$. We call this function k-rescaled. Thus we have $-\Delta\chi_i = E\chi_i$ everywhere inside Ω, with $\chi_i(k, \mathbf{r}) = 0$ on the rescaled boundary (*i.e.* for all

$k\mathbf{r}/k_i \in \Gamma$). The rescaled eigenfunction can be Taylor expanded in ω_i,

$$\begin{aligned}\chi_i(k,\mathbf{r}) &= \phi_i\left(\mathbf{r}+\frac{\omega_i}{k_i}\mathbf{r}\right) = \phi_i(\mathbf{r}) + \frac{\omega_i}{k_i}\mathbf{r}\cdot\nabla\phi_i + O(\omega^2) \\ &= \frac{\omega_i}{k_i} r_n \mathbf{n}\cdot\nabla\phi_i + O(\omega^2) \qquad \text{for } \mathbf{r}\in\Gamma, \end{aligned} \tag{46}$$

where Dirichlet boundary conditions were applied. We construct a basis of N functions $\xi_l(k,\mathbf{r})$, satisfying $-\Delta\xi_l = E\xi_l$ inside Ω, no particular boundary conditions on Γ, and non-orthogonal over Ω. We assume they approximately span the linear space in which rescaled eigenfunctions live, so that

$$\chi_i(k,\mathbf{r}) = \sum_{l=1}^{N} X_{li}\,\xi_l(k,\mathbf{r}) + \epsilon_i(\mathbf{r}) \qquad \text{for all } i \text{ of interest}, \tag{47}$$

where the error ϵ_i can be made negligibly small for some N. In practise N need exceed N_{sc} defined in (32) by only a small factor (2 or less). Our goal is then to solve for a shift ω_i and the corresponding i^{th} column of the coefficient matrix X. We can do this by simultaneous diagonalization of quadratic forms. We define two symmetric bilinear forms on the boundary,

$$f(u,v) := \oint_\Gamma \frac{1}{r_n} uv\, d\mathbf{s}, \tag{48}$$

$$g(u,v) := \frac{1}{k}\oint_\Gamma \frac{1}{r_n}(u\mathbf{r}\cdot\nabla v + v\mathbf{r}\cdot\nabla u)\, d\mathbf{s}. \tag{49}$$

Note that defining these forms brings the extra requirement that the domain be strictly star-shaped about the origin ($r_n > 0$), which from now on we assume. In the rescaled eigenbasis f is, via (46) and (45)

$$f(\chi_i,\chi_j) = \frac{\omega_i\omega_j}{k_i k_j} Q_{ij} + O(\omega^3) = 2\omega_i^2\delta_{ij} + O(\omega^3), \tag{50}$$

a matrix which is close to diagonal, because of the closeness of Q to the identity. In the same basis, recognizing that for k-rescaled functions g is equivalent to df/dk, the derivative of (49) with respect to the center wavenumber, and using $d\omega_i/dk = 1$, we have

$$g(\chi_i,\chi_j) = \frac{\omega_i+\omega_j}{k_i k_j} Q_{ij} + O(\omega^2) = 4\omega_i\delta_{ij} + O(\omega^2), \tag{51}$$

so g is also close to diagonal. Thus the set $\{\chi_i\}$ with small $|\omega_i|$ approximately diagonalizes both bilinear forms, with the approximation error growing as a power of $|\omega_i|$. As we explain below, in practise the converse applies, that is, by simultaneously diagonalizing f and g we can extract the set of eigenfunctions $\{\chi_i\}$ with smallest $|\omega_i|$. Therefore, loosely speaking, when the boundary weight function $1/r_n$ is used, domain eigenfunctions are given by the simultaneous eigenfunctions of the (squared) boundary norm and its k-derivative.

We perform the diagonalization in the basis (47). That is, matrices $F_{lm} := f(\xi_l, \xi_m)$ and $G_{lm} := g(\xi_l, \xi_m)$, with $l, m = 1 \cdots N$, are filled. This requires basis and first derivative evaluations on the boundary. It is an elementary fact that given a positive matrix F and a symmetric matrix G there exists a square matrix Y and a diagonal matrix $D := \mathrm{diag}\{\mu_i\}$ which satisfy $Y^T F Y = I$ and $Y^T G Y = D$. The matrices Y and D can be found by standard numerical diagonalization algorithms in $O(N^3)$ time. If (50) and (51) held without error terms, and the number of levels i for which they held were equal to (or exceeded) the basis size N, then we would be able directly to equate the columns of Y with the desired columns of X (barring permutations). In this case $\omega_i = 2/\mu_i$ would also hold, from which the desired wavenumbers k_i follow. However, using Weyl's law and (32) is follows that such a large number of levels requires that the largest $|\omega_i|$ is of order unity, in which case errors in (50) and (51) would become unacceptable. It is an empirical observation found through numerical study that in fact columns of Y corresponding to the *largest magnitude* generalized eigenvalues μ_i (and therefore the smallest shifts $|\omega_i|$) do accurately match columns of X. Thus perturbations by other vectors in the span of basis functions are small. Further discussion is postponed to a future publication [11].

We mention a couple of other implementation details. Because the generalized eigenproblem turns out to be singular it is truncated to its non-singular part [54, 7]. If columns of Y are normalized such that $Y^T F Y = I$ holds then the resulting eigenfunctions can be normalized over Ω by dividing the i^{th} column of Y by $\sqrt{2}\omega_i$. Depending on the choice of basis, spurious solutions can result; they are easily identified because their norm over Ω, easily found via the Rellich-type identity (discussed in [10])

$$\int_\Omega u^2 \, d\mathbf{r} \;=\; \frac{1}{2E} \oint_\Gamma r_n (u_n)^2 \, d\mathbf{s}, \tag{52}$$

is not close to 1. The maximum $|\omega_i|$ in which levels of useful accuracy are found is of order $0.2/R$ where R is the largest radius of the domain. The lack

of missing levels obtained with this method is illustrated by Fig. 5. There are several implementation issues and improvements that we do not have space to discuss here [54, 7, 11].

A word about the basis set choice $\{\xi(k, \mathbf{r})\}$, $1 \leq i \leq N$, is needed. Until now plane waves (including evanescent plane waves [54]) or regular Bessel functions [18] have been used. These fail for non-convex domain shapes, or those with corners, thus to tackle the domain in this study a basis of irregular Bessel (*i.e.* Neumann) functions, placed at equal intervals along a curve Γ^+ exterior to Ω, was developed by the author. Γ^+ is defined as the set of points whose nearest distance to Γ is D, with $kD = 7$ (roughly one wavelength distant). This was found to handle (non-reentrant) corners successfully. It performs extremely well for all shapes that have been attempted so far. The basis size N is about $1.5N_{\text{sc}}$ (see (32)), thus, depending on required accuracy, about $N/20$ useful levels are found per dense matrix diagonalization ($O(N^3)$ effort). This is $O(N)$ faster than other boundary methods; we remind the reader that N is larger than 10^3 in our work.

References

[1] O. Agam and S. Fishman, "Semiclassical criterion for scars of wavefunctions in chaotic systems", Phys. Rev. Lett. **73** 806–809 (1994).

[2] R. Aurich and M. Taglieber, "On the rate of quantum ergodicity on hyperbolic surfaces and for billiards", Physica D **118**, 84–102 (1998).

[3] E. J. Austin and M. Wilkinson, "Distribution of matrix elements of a classicaly chaotic system", Europhys. Lett. **20**, 589–593 (1992).

[4] A. Bäcker, R. Schubert, and P. Stifter, "On the number of bouncing ball modes in billiards", J. Phys. A, **30**, 6783–95 (1997).

[5] A. Bäcker, R. Schubert, and P. Stifter, "Rate of quantum ergodicity in Euclidean billiards", Phys. Rev. E **57**, 5425–47 (1998); also see Errata for this paper, Phys. Rev. E **58** (4) (1998).

[6] A. Bäcker, "Numerical aspects of eigenvalue and eigenfunction computations for chaotic quantum systems", in *The Mathematical Aspects of Quantum Maps*, M. Degli Esposti and S. Graffi (Eds.) Springer Lecture Notes in Physics 618, 91-144 (2003).

[7] A. H. Barnett, Ph. D. thesis, Harvard University, 2000.

[8] A. H. Barnett, D. Cohen, and E. J. Heller, Phys. Rev. Lett. **85**, 1412 (2000).

[9] A. H. Barnett, D. Cohen, and E. J. Heller, Rate of energy absorption for a driven chaotic cavity", J. Phys. A **34**, 413–437 (2001).

[10] A. H. Barnett, "Quasi-orthogonality on the boundary for Euclidean Laplace eigenfunctions", preprint.

[11] A. H. Barnett, "The scaling method for the Laplace eigenproblem", in preparation.

[12] M. V. Berry, "Regular and irregular semiclassical wavefunctions", J. Phys. A **10** 2083–91 (1977).

[13] M. V. Berry, in "Les Houches Lecture Notes, Summer School on Chaos and Quantum Physics" (M.-J. Giannoni, A. Voros, and J. Zinn-Justin, Eds.), Elsevier Science, Amsterdam, 1991; M. V. Berry, Proc. Roy. Soc. A **243** 219 (1989).

[14] E. B. Bogomolny, "Smoothed wave functions of chaotic quantum systems", Physica D **31**, 169–189 (1988).

[15] E. B. Bogomolny, B. Georgeot, M. Giannoni, and C. Schmidt, "Chaotic billiards generated by arithmetic groups", Phys. Rev. Lett. **69**, 1477–80 (1992).

[16] O. Bohigas, "Random matrix theories and chaotic dynamics", in *Chaos et physique quantique* (Les Houches, 1989), 87–199, M. J. Giannoni, A. Voros, and J. Zinn-Justin, eds, (North-Holland, Amsterdam, 1991).

[17] D. Boosé and J. Main, "Distributions of transition matrix elements in classically mixed quantum systems", Phys. Rev. E **60**, 2813–44 (1999).

[18] G. Casati and T. Prosen, "The quantum mechanics of chaotic billiards", Physica D **131**, 293–310 (1999).

[19] D. Cohen, Ann. Phys. (N.Y.) **283**, 175 (2000).

[20] D. Cohen, A. H. Barnett, and E. J. Heller, "Parametric evolution for a deformed cavity", Phys. Rev. E **63**, 046207 (2001).

[21] Y. Colin de Verdière, "Ergodicité et fonctions propres du laplacien", Comm. Math. Phys. **102** 497 (1985).

[22] M. Combescure and D. Robert, "Distribution of matrix elements and level spacings for classically chaotic systems", Ann. Inst. Henri Poincaré. **61**, 443 (1994).

[23] M. Combescure and D. Robert, "Semiclassical sum rules and generalized coherent states", J. Math. Phys. **36**, 6596–6610 (1995).

[24] H. Donnelly, "Quantum Unique Ergodicity", Proc. Am. Math. Soc. **131**, 2945–51 (2003).

[25] B. Eckhardt, S. Fishman, J. Keating, O. Agam, J. Main, and K. Müller, "Approach to ergodicity in quantum wave functions", Phys. Rev. E **52**, 5893–5903 (1995).

[26] F. Faure, S. Nonnenmacher, and S. De Bièvre, "Scarred eigenstates for quantum cat maps of minimal periods", Comm. Math. Phys. **239** 449–492 (2003).

[27] M. Feingold and A. Peres, "Distribution of matrix elements of chaotic systems", Phys. Rev. A, **34**, 591 (1986).

[28] C. V. Gardiner, *Handbook of Stochastic Methods for physics, chemistry, and the natural sciences*, 2nd Ed. (Springer-Verlag, 1997).

[29] M. C. Gutzwiller, *Chaos in Classical and Quantum Mechanics*, (Springer, NY, 1990).

[30] E. J. Heller, "Bound-state eigenfunctions of classically chaotic hamiltonian systems: scars of periodic orbits", Phys. Rev. Lett. 1515–18 (1984).

[31] E. J. Heller, "Wavepacket dynamics and quantum chaology", in *Chaos et physique quantique* (Les Houches, 1989), 547–664, M. J. Giannoni, A. Voros, and J. Zinn-Justin, eds, (North-Holland, Amsterdam, 1991).

[32] L. Hörmander, *The Analysis of Linear Partial Differential Operators III* (Springer, Berlin, 1985).

[33] S. Hortikar and M. Srednicki, "Random matrix elements and eigenfunctions in chaotic systems", Phys. Rev. E **57**, 7313–16 (1998).

[34] J. R. Kuttler and V. G. Sigillito, "Eigenvalues of the Laplacian in two dimensions", SIAM Review, **26**, 163–193 (1984).

[35] B. Li and B. Hu, J. Phys. A **31**, 483 (1998).

[36] E. Lindenstrauss, "Invariant measures and arithmetic quantum unique ergodicity", preprint.

[37] W. Luo and P. Sarnak, preprint (2004).

[38] A. Martinez, *An Introduction to Semiclassical and Microlocal Analysis*, (Springer, 2002).

[39] L. Kaplan and E. J. Heller, "Linear and nonlinear theory of eigenfunction scars", Ann. Phys. **264**, 171–206 (1998).

[40] L.Kaplan and E. J. Heller, "Measuring scars of periodic orbits", Phys. Rev. E **59**, 6609–28 (1999).

[41] S. W. McDonald and A. N. Kaufman, Phys. Rev. Lett. **42**, 1189–92 (1979).

[42] T. Prosen, "Statistical properties of matrix elements in a Hamilton system between integrability and chaos", Ann. Phys. N.Y. **235**, 115–164 (1994).

[43] T. Prosen, "Quantization of a generic chaotic 3D billiard with smooth boundary. I. Energy level statistics", Phys. Lett. A **233**, 323–331 (1997); T. Prosen, "Quantization of a generic chaotic 3D billiard with smooth boundary. II. Structure of high-lying eigenstates", Phys. Lett. A **233**, 332–342 (1997).

[44] Z. Rudnick and P. Sarnak, "The behaviour of eigenstates of arithmetic hyperbolic manifolds", Comm. Math. Phys. **161** 195–213 (1994).

[45] P. Sarnak, "Arithmetic quantum chaos", The Schur lectures (Tel Aviv, 1992), Israel Math. Conf. Proc. **8**, 183–236 (Bar-Ilan University, 1995).

[46] P. Sarnak, "Spectra of Hyperbolic Surfaces", Bulletin of the AMS, **40**, 441–478 (2003).

[47] H. Schanz and T. Kottos, "Scars on quantum networks ignore the Lyapunov exponent", Phys. Rev. Lett. **90**, 234101 (2003).

[48] A. I. Schnirelman, Usp. Mat. Nauk. **29**, 181 (1974).

[49] Ya. G. Sinai, "Dynamical systems with elastic reflections: ergodic properties of dispersing billiards", Russ. Math. Surveys **25**, 137–189 (1970).

[50] D. S. Sivia, *Data Analysis: A Bayesian Tutorial*, (Oxford, 1996).

[51] F. Steiner, `chao-dyn/9402001` (1994).

[52] G. Tanner, "How chaotic is the stadium billiard? A semiclassical analysis", J. Phys. A **30**, 2863–88 (1997).

[53] G. Veble, M. Robnik, and J. Liu, "Study of regular and irregular states in generic systems", J. Phys. A **32**, 6423–44 (1999).

[54] E. Vergini and M. Saraceno, Phys. Rev. E, **52**, 2204 (1995); E. Vergini, Ph. D. thesis, Universidad de Buenos Aires, 1995.

[55] M. Wilkinson, "A semiclassical sum rule for matrix elements of classically chaotic systems", J. Phys. A **20**, 2415–23 (1987).

[56] S. Zelditch, "Uniform distribution of eigenfunctions on compact hyperbolic surfaces", Duke Math. J. **55**, 919 (1987).

[57] S. Zelditch, "Quantum transition amplitudes for ergodic and for completely integrable systems", J. Funct. Anal. **94**, 415–436 (1990).

[58] S. Zelditch and M. Zworski, "Ergodicity of eigenfunctions for ergodic billiards", Comm. Math. Phys., **175** 673–682 (1996).

[59] S. Zelditch, "Note on Quantum Unique Ergodicity", *to appear*, Proc. AMS, `math-ph/0301035` (2003).